

ANALYSIS OF WELDING FAILURE OF AMMONIA SYNTHESIS CONVERTOR

A DISSERTATION

*submitted in partial fulfilment of the
requirements for the award of the degree*

of

MASTER OF ENGINEERING

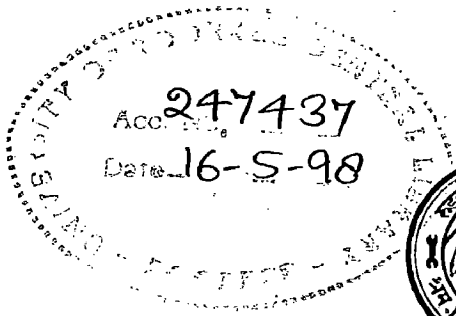
in

METALLURGY ENGINEERING

(With Specialization in Industrial Metallurgy)

By

DHEERAJ MOHAN MODAWEL



**DEPARTMENT OF METALLURGY ENGINEERING
UNIVERSITY OF ROORKEE
ROORKEE-247667 (INDIA)**

MAY, 1996

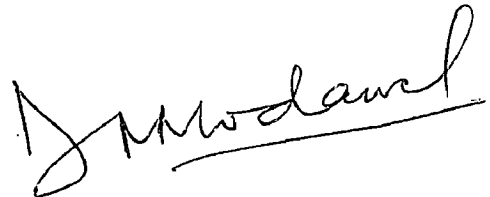
CANDIDATE'S DECLARATION

I hereby declare that the work which is being presented in the dissertation entitled "**ANALYSIS OF WELDING FAILURE OF AMMONIA SYNTHESIS CONVERTOR**" in partial fulfillment of the requirements for the award of the degree of "**Master of Engineering**" in Metallurgy Engineering with specialisation in "**Industrial Metallurgy**", submitted in the Department of Metallurgy, University of Roorkee, Roorkee is an authentic record of my own work carried out over a period of five months from 1st October 1994 to 10th November 1994 and then from 15th January 1996 to 23th May 1996, under the supervision of **Dr. M. L. Kapoor**, Professor, **Dr. P. S. Mishra**, Professor and Head, Department of Metallurgy Engineering, University of Roorkee, Roorkee, and **Shri C.P. Chhabra**, Manager, E.T.S., Tata Chemicals Ltd., Babrala.

The matter embodied in this dissertation has not been submitted by me for the award of any other degree.

PLACE : Roorkee

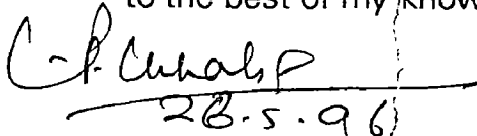
DATE : 28.05.96



(DHEERAJ MOHAN MODAWEL)

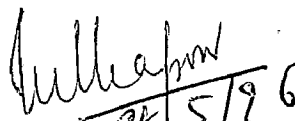
CERTIFICATE

This is to certify that the above statement made by the candidate is correct to the best of my knowledge and belief.



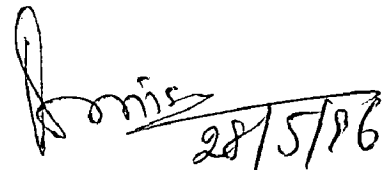
(Er. C.P. Chhabra)

Manager, ETS
Tata Chemicals Ltd.
Babrala



(Dr. M. L. Kapoor)

Professor
Dept. of Metallurgy Engg.
University of Roorkee
Roorkee



(Dr. P. S. Mishra)

Professor & Head
Dept. of Metallurgy Engg.
University of Roorkee
Roorkee

ACKNOWLEDGEMENT

I wish to express my deep sense of gratitude to **Dr. P.S. MISHRA**, Professor & Head, Metallurgy Engineering Department, **Dr. M.L. KAPOOR**, Professor, Metallurgy Engineering Department, University of Roorkee, Roorkee and **Shri C.P. CHHABRA**, Manager (ETS), TATA CHEMICALS LIMITED, BABRALA, for their constant guidance and valuable suggestions during the course of this work. The present form of the work would have been very difficult to achieve without their constant available help.

Heart felt gratitude is extended to **Dr. V.K. Tiwari**, Professor, Metallurgy Engineering Department, for his kind help and dynamic cooperation.

Heartfelt thanks are also due to **Shri G.P. Khurana**, President, TCL, Babrala and to **Shri P.J. Pareek**, Vice President, TCL, Babrala for their generous support and encouragement throughout this work.

I would like to thanks all the technicians and workers of Metallurgy Engineering Department, who were directly or indirectly involved in this work.

Sincere thanks are extended to Shri N. Rastogi, Mr. S. K. Bhatt, Mr. Asheesh Srivastava, Mr. Alok Kansal, Mr. Arvind Jain, Mr. Akhilesh Bandale and Mr. S.K. Srivastava, for their encouragement and valuable suggestions throughout this work.

Last but not the least, author happily acknowledges the encouragement and cooperation extended by his Bhaiya and Bhabhi.

PLACE : Roorkee

DATE : 23.05.96


(DHEERAJ MOHAN MODAWEL)

ABSTRACT

This work is an attempt to find the reasons which have lead to cracking of weld seam no. 6 of **Ammonia Synthesis Convertor** of Tata Chemicals Limited, Babrala. Failure of convertor occurred after six months of service in hydrogen atmosphere.

Microstructure of the weld metal showed some amount of abnormalities in the region where cracks were observed. Coarse carbides and coarse prior austentic grains were observed, in the weld metal. Hardness of the weld metal was found exceeding the safe limits of 250 HV, in the region where cracks were observed. These abnormalities were found to be due to incorrect post weld heat treatment, which have resulted in hydrogen induced cracking (HIC).

LIST OF FIGURES

FIGURE NO.	TITLE	PAGE NO.
Fig. 2.1	Fractograph showing dimpled pattern typical of overstress fractures of ductile metals or alloys.	40a
Fig. 2.2	Fractograph showing a cleavage facet containing river marks generated by a sub-grain boundaries.	40a
Fig. 2.3	Fractograph showing brittle fracture in steel that resulted from stress - corrosion cracking. Showing an absence of deformation.	40a
Fig. 2.4	Sequence of occurrence of fractures.	40b
Fig. 3.1	Variation of 10^5 - h creep rupture strength as a function of temperature for various Cr-Mo steel.	41
Fig. 3.2	Effect of elevated temperature exposure on the room temperature tensile properties of normalised 0.17% steel after exposure.	42
Fig. 3.3	Schematic of changes in creep strengthening contributions at 550°C in normalised and normalised & tempered Mo steel.	43
Fig. 3.4	Hardness as a function of carbon percentage for various microstructure.	43
Fig. 3.5	Decrease in hardness with increasing tempering temperature for various carbon contents.	44
Fig. 3.6	Relationship between change in creep rate and change in room temperature hardness during creep of normalised 1% Mo steel tested at 123 MPa at 550°C.	44

Fig. 3.7	Influence of heat treatment on 10^5 hr creep rupture strength of 2.25% Cr - 1% Mo steel.	45
Fig. 3.8	Retardation of softening and secondary hardening during tempering of steels with various molybdenum contents.	45
Fig. 3.10	Effect of test temperature on strength of 2 $\frac{1}{4}$ Cr - 1 Mo steel.	46
Fig. 3.11	Effect of test temperature on ductility of 2 $\frac{1}{4}$ Cr - 1 Mo steel.	46
Fig. 3.12	Effect of strain rate on elevated temperature tensile strength of 2 $\frac{1}{4}$ Cr - 1 Mo steel.	46
Fig. 3.13	Effect of Chromium content on tensile and yield strength of Cr - Mo steel.	47
Fig. 3.14	Effect of chromium on creep strength of steel containing Mo, Si & Al at 540°C.	48
Fig. 3.15	Isothermal diagram showing the sequence of carbide formation of tempering of normalised 2 $\frac{1}{4}$ Cr - 1 Mo steel.	48
Fig. 3.16	CCT diagram for air cooled 2 $\frac{1}{4}$ Cr - 1 Mo steel.	49
Fig. 3.17	TTT diagram of 2.16 Cr - 0.96 Mo steel.	50
Fig. 3.18	Thermal conductivity of carbon and alloy steels at various temperature.	51
Fig. 4.1	Physical and chemical processes necessary for various types of hydrogen embrittlement.	52
Fig. 5.1	Ammonia Synthesis convertor.	53
Fig. 5.2	Ammonia plant process diagram.	54

Fig. 5.3	Intermediate stress relieving cycle.	55
Fig. 5.4	Post weld heat treatment.	56
Fig. 5.5	Positions are marked on the weld seam for taking the hardness at various location.	57
Fig. 5.6	Weld seam showing the location of various zones for further analysis.	58
Fig. 5.7	Cracks following course prior austentic grain boundaries. Porosity is also visible (unetched; X 30).	59
Fig 5.8	Same as 5.7, but at higher magnification (unetched; X 100).	59
Fig. 5.9	Cracks following course prior austentic grain boundaries. Porosity is also visible (unetched; X 30).	60
Fig. 5.10	Same as Fig. 5.8, but this time after etched in nital (X 100).	60
Fig. 5.11	Micrograph showing crack initiating zone where coarse austenitic grains are visible (Etched in nital; X 100).	61
Fig. 5.12	Micrograph away from the crack showing fine prior austenitic grains as compared to coarse grain shown in Fig. 5.11 (Etched in nital; X 100).	61
Fig. 5.13	Microstructure of HAZ and weld metal, showing orientation of columnar grains (Etched in nital; X 30).	62
Fig. 5.14	Microstructure of HAZ and parent metal, showing orientation of columnar grains (Etched in nital; X 30).	62
Fig. 5.15	Microstructure of parent metal showing carbide precipitation (Etched in nital; X 30).	63

Fig. 5.16	Microstructure of parent metal showing carbide precipitation (Etched in nital; X 100).	63
Fig. 5.17	Fractograph showing mixture of intergranular cracks, dimple features, tearing & cleavage which has resulted in failure.	64
Fig. 5.18	Fractograph showing considerable amount of dimples formed by microvoid coalescence.	64
Fig. 5.19	Crack apparently has propagated by mixed mechanism - dimple rupture, intergranular with some evidence of transgranular cracking, and predominant tearing.	65
Fig. 5.20	Columnar grains and equiaxed grains. Cracking has occurred mainly by dimple rupture with some sign of tear ridges.	65
Fig. 5.21	Enlarged view of Fig. 5.20. This portion of fracture shows transgranular cracks, deep secondary cracks, and hair line indication. Visible are fine ridges, typical of hydrogen embrittlement.	66
Fig. 5.22	Intergranular cracks with deep secondary cracks between the columnar grains.	66
Fig. 5.23	Structure variation observed along the cracked regions. It shows the ductile portion of the fracture surface. At the lower portion, microvoid coalescence is visible.	67
Fig. 5.24	Enlarged view of the bottom portion of Fig. 5.23. Channeling which has occurred due to coalescence of voids is visible, surrounded by large tear ridges, secondary cracks are also visible.	67

Fig. 5.25	Fractograph showing columnar grains and equiaxed grains. Cracking has occurred mainly by dimples rupture in this region.	68
Fig. 5.26	Enlarged view of Fig. 5.24, showing channeling which has occurred due to micro - void coalescence. It also shows large tear ridges.	68
Fig. 5.27	Standard sample piece for toughness test (Charpy test).	69
Fig. 5.28	Standard tensile test specimen.	70
Fig. 5.29	Microstructure of defect free zone (i.e. C ₁ zone), showing tempered martensite with some amount of retained austenite (Etched in nital; X 1000).	71
Fig. 5.30	Same as 4.29 but at different location (Etched in nital; X 1000)	71
Fig. 5.31	Micrograph of weld zone showing quenched and tempered martensite structure of C ₁ zone (Etched in nital; X 1000).	72
Fig. 5.32	Fractured surface of sample piece taken from A ₁ zone for SEM analysis.	76
Fig. 5.32 A	Stress-strain curve of transverse piece (Zone B ₁)	73
Fig. 5.33	A ₁ zone of weld seam, where cracks were observed. Photograph is taken after Dye penetration test. Twenty distinct radial cracks are visible (Photograph by the courtesy of TCL, Babrala).	77
Fig. 5.33 A	Stress-strain curve of longitudinal piece (Zone B ₁)	74
Fig. 5.34	Same as Fig. 5.33, but different view.	78
Fig. 5.34 A	Nelson Curve.	75

Fig. 5.35	Top portion of the segment of weld seam taken from A ₁ zone Radial cracks are visible (Photography by the courtesy of TCL, Babrala).	79
Fig. 5.36	Photograph of the segment of circumferential weld seam showing its inner dia with clear visible longitudinal cracks (Photography by the courtesy of TCL, Babrala).	80
Fig. 5.37	Photograph of the segment of weld seam taken from internal reactor surface showing longitudinal and transverse cracks (Photography by the courtesy of TCL, Babrala).	81
Fig. 5.38	Top portion of the segment of weld seam from A ₁ zone. Showing twenty radial cracks (Photography by the courtesy of TCL, Babrala).	82

LIST OF TABLES

TABLE No.	TITLE	PAGE NO.
Table 3.1	Nominal chemical composition of chromium molybdenum steel.	83
Table 5.1	Composition of synthesis gas which enters NH ₃ synthesis convertor.	84
Table 5.2	Hardness values obtained from outside the convertor.	85
Table 5.3	Hardness values obtained from inside the convertor.	86
Table 5.4	Hardness values of transverse and longitudinal samples taken from zone B ₁ .	87
Table 5.5	Results of charphy test performed on sample piece taken from B ₁ zone.	88
Table 5.6	Tensile test for B ₁ zone.	89
Table 5.7	Chemical analysis report of samples of various zones.	90
Table 5.8	Hardness values of sample piece taken from C ₁ zone.	91
Table 5.9	Room temperature mechanical properties of 2.25% Cr - 1% Mo steel.	92
Table 5.10	Standard chemical composition of A 387 Gr. 22 Cl. 2 plates as per ASTM standards.	92

CONTENTS

	CANDIDATE'S DECLARATION	(i)
	ACKNOWLEDGEMENT	(ii)
	ABSTRACT	(iii)
	LIST OF FIGURES	(iv)
	LIST OF TABLES	(ix)
CHAPTER 1	INTRODUCTION	1
	1.1 INTRODUCTION OF CR-MO STEEL	1
	1.2 HYDROGEN EMBRITTLEMENT IN CR-MO STEEL	2
	1.3 ABOUT THE REPORT	3
CHAPTER 2	FAILURE ANALYSIS - AN APPROACH	5
	2.1 INTRODUCTION	5
	2.2 STAGES OF FAILURE ANALYSIS	5
	2.2.1 History of the failed equipment	6
	2.2.2 Preliminary examination of the Failed Parts	7
	2.2.3 Non destructive testing	7
	2.2.4 Selection, Preservation and cleaning of fracture surface.	8
	2.2.5 Macroscopic examination of fractured surface	8
	2.2.6 Microscopic examination of fractured surface	9
	2.2.7 Determination of fractured type	9
CHAPTER 3	LITERATURE REVIEW-I (CHROMIUM MOLYBDENUM STEEL)	11
	3.1 INTRODUCTION	11
	3.2 FACTORS AFFECTING MECHANICAL PROPERTIES	12
	3.2.1 Strengthening Mechanism	12
	3.2.2 Effects of Microstructure	15
	3.2.3 Effects of Heat Treatment	16
	3.2.4 Effects of Compositions	16
	3.3 WELDING METALLURGY	19

	3.4	DEGRADATION OF MECHANICAL PROPERTIES DUE TO LONG-TERM ELEVATED TEMPERATURE EXPOSURE	21
CHAPTER	4	LITERATURE REVIEW - II (HYDROGEN INDUCES CRACKING)	22
	4.1	INTRODUCTION	22
	4.2	HYDROGEN EMBRITTLEMENT	22
	4.3	FACTORS AFFECTING HIC	25
		4.3.1 Effects of Hydrogen	25
		4.3.2 Role of Stress	25
		4.3.3 Role of Microstructure	26
	4.4	HYDROGEN CRACKING IN WELDMENTS	26
	4.5	FEATURES OF HIC IN SEM	28
CHAPTER	5	ANALYSIS OF WELDING FAILURE - A CASE STUDY	29
	5.1	FAILURE ANALYSIS REPORT	29
		5.1.1 Introduction of the Equipment	29
		5.1.2 Welding Procedure Followed	30
	5.2	HISTORY OF AMMONIA SYNTHESIS CONVERTOR	30
	5.3	PRELIMINARY EXAMINATION OF THE WELD SEAM	31
	5.4	SAMPLE FOR FURTHER ANALYSIS	32
		5.4.1 Weld Seam Zone A₁	32
		5.4.2 Weld Seam Zone B₁	34
		5.4.3 Weld Seam Zone C₁	36
		RESULTS AND DISCUSSION	37
		REFERENCES	

1.1 INTRODUCTION OF Cr - Mo STEEL

Cr-Mo steels are widely used in oil refineries, chemical industries and electrical power generating stations for piping, heat exchangers, superheater tubes and pressure vessels. The main advantage of these steels is the improved creep strength from molybdenum and chromium addition, and enhanced corrosion resistance from chromium. The creep strength of Cr-Mo steels is derived mainly from two sources, solid solution strengthening of the matrix ferrite by carbon, molybdenum and chromium, and precipitation hardening by carbides[2].

Cr-Mo steel with chromium ranging from 0.5 - 9.0 % and molybdenum ranging for 0.5 - 1.0% are often used upto 650°C without the presence of hydrogen or upto 480°C in hydrogen environment.

Selection of steels to be used at elevated temperatures generally involves a compromise between the higher efficiencies obtain at higher temperature and the cost of equipment including material, fabrication, replacement and downtime costs. The highly alloyed steels, which depend on an austenitic matrix for their high temperature properties, generally have higher resistance to mechanical and chemical degradation at elevated temperature than the low alloy ferrite steel. However, a higher alloy content generally means higher cost. Therefore, carbon and low alloy ferritic steels are extensively used in several forms (piping, pressure vessel plates, bolts, structural parts) in a variety of application that involves exposure to elevated temperature. In addition, interest in ferritic steels have

increased recently because of their relatively low thermal expansion coefficient and high thermal conductivity, which make them more attractive than austenitic steels in applications where thermal cycling is present [2].

The weldability of Cr-Mo steel is very similar to that of quenched and tempered and hardenable low alloy steel. The major problem in the HAZ is cracking in the hardened coarse-grain region, as well as HAZ softening between A_{c1} and A_{c3} . Reheat cracking during post weld heat treatment (PWHT) and long term exposure in elevated temperature service condition also can cause severe problems. The appropriate preheat and interpass temperature should be selected and low hydrogen practice should be used, while welding such steel to avoid cracking [13a].

Post weld heat treatment is required for Cr - Mo steel which has Cr% more than 1.25 and whose thickness is more than 12 mm.

The post weld heat treatment (PWHT) of the Cr-Mo weldments is also referred to as stress relieving heat treatment. This process helps to relieve residual stress and temper as welded hardened microstructure to improve the fracture toughness of HAZ and weld metal. Additional beneficial effect of PWHT is to allow for more dissipation of hydrogen in the weld region so that the chances of hydrogen-induced cold cracking is further reduced.

1.2 HYDROGEN EMBRITTLEMENT IN CR - MO STEEL

Cr-Mo steel are susceptible to hydrogen cracking if care is not taken to avoid it. Susceptibility of ferritic steel (Cr-Mo steel) to HIC is due to low solubility and high diffusivity of hydrogen in ferrite. Though the solubility of hydrogen in ferrite is negligible at room temperature it increases almost linearly with

temperature upto $\alpha \rightarrow \gamma$ transformation temperature, where the solubility approximately doubles abruptly from about 3 to 6.5 ppm and continues to increase in a more rapid linear fashion above this temperature and at the melting point it approximately doubles again from 14 to 26 ppm.

On lowering the temperature, there result a sharp decrease in solubility, which inturn results in supersaturated steel. Hence, dissolve hydrogen will diffuse out of the metal lattice and recombine to form molecular hydrogen, in the discontinuties like grain boundaries or voids. Due to this, pressure in the voids increase and makes the steel weaker.

1.3 ABOUT THE REPORT

This report is an attempt to investigate the failure of A387 Gr. 22 Cl. 2 steel which occured in hydrogen atmosphere after six months of service. Chapter 3 deals with Cr - Mo steel in detail. This chapter focuses on factors that affects mechanical properties of Cr-Mo steel, their weldability and effects of alloying element on the performance of these steels. Chapter 4 deals with the theories of hydrogen embrittlement and about the factors that helps HIC to occur. Chapter 2, focuses on general approach for any failure analysis. Chapter 5, describes a case study of weld failure of AMMONIA SYNTHESIS CONVERTOR which got cracked in service.

On analysis, it was found that weld seam was having excessive hardness especially in the region where cracks were found. Microstructure also shows some amount of flaws like porosity, coarse prior austenite grains, coarsening of carbides and even at some places these carbides have precipitated along the grain boundaries. Due to all these flaws it has resulted in hydrogen embrittlement of HIC type which has lead to cracking along weld seam.

During the initial stages of this project, we have two possibilities in mind for this failure, they were, either it has occurred due to faulty operating condition or there is some inherent fault in the weld metal. But the fact that cracks were found only in the weld metal, gave us some clue about the problem.

The possibility of high temperature hydrogen attack due to faulty operation was eliminated as there was no experimental evidence found to support it (cracks nucleated by such a phenomenon are accompanied by decarburization effects).

2.1 INTRODUCTION

Although the word failure bears the burden of negative connotation, the practice of failure analysis is above all else, the systematic pursuit to the positive - the pursuit of technological progress. It is a science dedicated to the principle that the extension of product improvement and reliability depends in large part on the recognition of shortcomings that can be usually be corrected and on the identification of problems that, when fully explored and understood can, usually be solved.

2.2 STAGES OF FAILURE ANALYSIS

Principle stages that comprise the investigation and analysis of a failure are as follows :-

1. Collection of the background data and selection of samples.
2. Preliminary examinations of the failed parts (visual and record keeping).
3. Non-destructive testing.
4. Mechanical testing (includes hardness and toughness)
5. Selection, identification, preservation and / or cleaning of all specimens.
6. Macroscopic examination and analysis (fracture surfaces, secondary cracks and other surface phenomena).
7. Microscopic examination and analysis.
8. Selection and preparation of metallographic sections.

9. Examination and analysis of metallographic sections.
10. Determination of failure mechanism.
11. Chemical analysis.
12. Analysis of fracture mechanics.
13. Testing under simulated conditions.
14. Analysis of all the evidence formulation of conclusions and writing the report (including recommendation)

The sequence as suggested above may be altered and some stages might be deleted depending upon the type of actual failure. It is worthwhile here to highlight some important aspect of such analysis.

2.2.1 HISTORY OF THE FAILED EQUIPMENT

Failure investigation should be directed towards gaining an acquaintance with all pertinent details related to the failure, collecting the available information regarding the manufacturing processing and service history of the failed component or structure.

To focus on history of the failed equipment we should focus on the following points in detail :-

- a) Service history
- b) Photographic records of failed components.
- c) Selection of samples for analysis.
- d) Wreckage analysis - To elaborate this point let us take one examples

in which problems involves the establishment of sequence of fracture so as to determine the origin of initial failure. Usually, the direction of the crack growth can

be detected from marks on the surface. The typical sequence of fractures is shown in fig. 2.4, where A and B represent fractures that intersect at a point. It is clear about the sequence of the cracks, fracture A must have occurred prior to fracture B because the presence of fracture A served to arrest fracture B. This method of sequencing is called T-junction procedure and is an important technique in wreckage analysis.

2.2.2 PRELIMINARY EXAMINATION OF THE FAILED PARTS

The failed parts, including all its fragments should be subjected to a thorough visual examination before any cleaning is undertaken, often soil or debris formed on the surface provide useful evidence in establishing the cause of failure or in determining a sequence of events. Preliminary examination includes,

- a) Visual Inspection.
- b) Photographing fractures.

2.2.3 NON DESTRUCTIVE TESTING

It is the essential tool in the field of failure analysis. The following NDT generally used are:

- a) Liquid Penetration test : For surface flaws
- b) Magnetic Particle test : Utilises magnetic field to locate surface and sub-surface discontinuities in ferromagnetic materials.
- c) Ultra sonic test : Utilises high frequency sound waves to detect minute cracks available in thick sections.
- d) Radiography : For internal variations and defects.

2.2.4 SELECTION, PRESERVATION AND CLEANING OF FRACTURE SURFACE

The proper selection, preservation and cleaning of fracture surfaces are vital to prevent important evidence from being destroyed or obscured. Following points should be followed to preserve surface :-

- 1) Care should be taken while removing the fracture surface from the fractured zone.
- 2) Cover the surface from cotton or cloth so as to avoid any damage during shipment.
- 3) Touching or rubbing the surface of the fracture with finger should definitely be avoided.
- 4) Desiccators should be used to preserve them from atmosphere degradation.

2.2.5 MACROSCOPIC EXAMINATION OF FRACTURED SURFACE

The amount of information that can be obtained from examination of the fracture surface is surprisingly extensive. Macroscopic examination of fracture surfaces may give an indication of the stress system that produced failure. Failure in monotonic tension produces a flat fracture normal to the maximum tensile stress under plane strain conditions and a slant (shear) fracture at about 45° if plane stress conditions prevail.

Macroscopic examination can usually determine the direction of crack growth and hence the origin of failure. With brittle flat fractures, determination depends largely on the fracture surface showing chevron marks. The direction of crack growth is almost always away from the tips of the chevrons. Chevron marks occur because nearly all cracks are stepped at an early stage in their

development and as the crack front expands the traces of the steps form chevron marks.

2.2.6 MICROSCOPIC EXAMINATION OF FRACTURED SURFACE

The interpretation of micro fractographs requires practice and understanding of fracture mechanisms there are only a small no of basic features that are clearly recognisable and indicative of a particular mode of failure. These are as follows :-

- 1) Dimples fractures are, typical of overstress failures of ductile metals and alloys (Refer figure 2.1).
- 2) Cleavage facets are, typical of transgranular brittle fracture of bcc and hcp metals and alloys (Refer figure 2.2).
- 3) Brittle inter-granular fracture typical of temper embrittlement steel, where fracture is due to segregation of an embrittling species at the grain boundaries, to intergranular stress corrosion cracking or to hydrogen embrittlement (Refer figure 2.3).

2.2.7 DETERMINATION OF FRACTURED TYPE

To determine the cause of fracture it is usually necessary to determine the type of fracture. Though a satisfactory logical classification of failures involving fracture does not exist, still one can think of the prominent features of each type of fracture.

A) Ductile Fracture

Some of the main features of ductile fracture are :-

- a) Neck formation resulting in cup and cone fracture.

- b) Ductile fracture involving shear stress components, generates elongated dimples. When these dimples are produced by a shear component, the dimples in the mating fracture surfaces point in opposite directions.

B) Transgranular brittle fracture

It is generally indicated by presence of transgranular cleavage in BCC and HCP metals and does not occur in the case of FCC metals and alloys. The prominent fractures of this fracture are as follows :-

- a) Presence of fan shaped cleavage plateaus having river marks in polycrystalline specimens.
- b) Presence of cleavage on conjugate planes.
- c) Ductile tears joining cleavage planes at different levels.

C) Intergranular Brittle Fracture

Some causes and indications of intergranular brittle fractures are as follows:-

- a) Presence of second phase particles (such as carbide in iron-nickel-chromium alloy) at the grain boundaries.
- b) Segregation of a specific element or compound to a grain boundary where a layer of few atoms thick is sufficient to cause embrittlement.

**LITERATURE REVIEW - I
(CHROMIUM - MOLYBDENUM STEEL)**

3.1 INTRODUCTION

The advantage like high creep resistance and good corrosion resistance along with a satisfactory resistance to oxidation in air of Cr-Mo steel (for composition refer table 3.1), were fully exploited by thermal & nuclear power plants and the fertiliser & petrochemicals plants.

The oxidation resistance and high temperature strength of these steels are functions of their chromium and molybdenum contents. Chromium contributes more to oxidation resistance, and molybdenum contribute more to high temperature strength. [9]

The use of austenitic steels in construction of power plant has been largely reduced primarily due to two reasons. After about 1960, it has become possible to operate power plant with a heat rate about 20% lower than that require to run the power plant in the early fifties [1]. Thus, the service condition has allowed to replace the expensive austenitic steels with ferritic steel in fabrication of high pressure systems. The use of austenitic stainless steels posing welding difficulties with corresponding increase in wall thickness. Ferritic steels have relatively lower thermal expansion coefficient and higher thermal conductivity (refer fig 3.18) makes them more suitable than austenitic steels in application where thermal cycling is present [2].

Cr- Mo steels are also used in the fabrication of extremely - large heavy - wall vessels for hydrotreating processes in the petroleum industry or for ammonia

synthesis in fertilizer plants. The Cr-Mo steels are required here to prevent damage to the vessel by the relatively high-pressure hydrogen it contains.

Both normalized & tempered and quenched & tempered steels are used in constructing these vessels. These treatment results in microstructure of low-carbon martensite or bainite. The absence of large quantities of carbides, however, results in greater ductility at any given strength level than that obtained from high carbon steels.

3.2 FACTORS AFFECTING MECHANICAL PROPERTIES

The factors affecting the mechanical properties of steels includes the nature of the strengthening mechanisms, the microstructure, the heat treatment, and the alloy composition.

In addition, various service factors such as thermal exposure and environmental conditions can induce metallurgical changes (refer fig 3.1 & fig.3.2), which may affect the mechanical properties of steels used at elevated temperatures. These metallurgical changes includes spheroidization. Depending on the temperature and exposure environment ferritic steels used at elevated temperatures may also be susceptible to embrittlement phenomena such as temper embrittlement, creep embrittlement, hydrogen embrittlement, and liquid-metal embrittlement [5, 6, 7, 8].

3.2.1 STRENGTHENING MECHANISM

The creep strength of a steel is affected by the typical strengthening mechanisms - namely grain refinement, solid solution hardening and precipitation hardening. Of these various strengthening mechanisms, the refinement of grain size is perhaps the most unique because it is the only strengthening mechanism

that also increases toughness [2].

The creep strength of chromium-molybdenum steels is mainly derived from a complex combination of solid solution and precipitation effects, as illustrated in figure 3.3. In the early stages of creep, solid solution effects are the largest contributor to creep resistance. As time progresses, the precipitation of carbides (primarily Mo_2C in the case of molybdenum steels) contributes more to the creep resistance.

Both these strengthening become ineffective at high temperatures. In solid-solution hardening, an increase in temperature increases the diffusion rates of solute atoms in the dislocation atmospheres while at the same time dispersing the atoms of the atmospheres, with both effects making it easier for dislocations to move. In precipitation hardening, heating of the alloy to an excessively high temperature can cause solutionizing of the precipitates. At intermediate temperatures, the precipitates can coarsen and become less-effective impediments to dislocation motion. High stresses and high strain cyclic loading also can lead to accelerated softening.

Solid-Solution strengthening

It occurs primarily from a process termed interaction solid-solution hardening (or strengthening), which is the mechanism that involves the interaction of substitutional and interstitial solutes. The process occurs in ferritic alloys that contain solid solution interstitial and substitutional elements that have an affinity for each other. As a result of this strong attraction, atom pairs or clusters could form dislocation atmospheres that hinder dislocation motion and therefore strengthens the steel [2].

Precipitation Strengthening

Precipitation strengthening is more significant in molybdenum steels, for which the strengthening precipitates are mainly Mo_2C and Mo_2N . Further, increase in precipitation strengthening can be achieved with additions of niobium or vanadium to chromium-molybdenum steels. The stability of the carbides increases in the following order of alloying elements : chromium molybdenum, vanadium and niobium [2, 4].

Secondary Hardening

If the mechanical properties of tempered steels need to be maintained at elevated service temperatures, the problem is to reduce amount of softening during tempering so that higher strength can be achieved at higher temperatures. One way to reduce softening is with strong carbide formers such as chromium, molybdenum and vanadium. These carbide formers induce an effect known as secondary hardening. Without these elements, iron carbon alloys and low carbon steels soften rapidly with increasing tempering temperature, as shown in figure 3.5. If present in sufficient quantity, however, the carbide-forming elements not only retard softening but also form fine alloy carbides that produce a hardness increase at higher tempering temperatures. This hardness increase is frequently referred to as secondary hardening [2]. This hardening can also occur during elevated temperature service and is related to creep strength, as shown in figure 3.6 .

Secondary hardening allows higher tempering temperatures, and this increases the range of service temperatures. Figure 3.8 shows secondary hardening in a series of steels containing molybdenum. The secondary hardening peaks develop only at high tempering temperatures because alloy carbide

formation depends on the diffusion of the carbide-forming elements, a more sluggish process than that of carbon and iron diffusion. As a result, not only is a finer dispersion of particles produced but also the alloy carbides, once formed, are quite resistant to coarsening. Due to this reason, chromium-molybdenum steels are used for the fabrication of pressure vessels and reactors for service temperature around 500° centigrade. The intensity of secondary hardening can be increased by increasing the mismatch between the carbides precipitate and the matrix [2]. Increasing mismatch is produced by :-

- increasing the lattice parameter of the carbide precipitate.
- decreasing the lattice parameter of the matrix.

3.2.2 EFFECTS OF MICROSTRUCTURE

It is widely accepted that the strength and impact toughness of carbon and chromium-molybdenum steels with fully bainitic microstructures are better than those with a ferritic-bainitic microstructures, they also have better creep resistance under high stress, short-time conditions, but degrade more rapidly at high temperatures than pearlitic structures. Moreover, even though bainitic microstructures improves strength, toughness, and creep resistance, chromium molybdenum steels with bainitic and tempered martensitic microstructures also undergo strain softening during mechanical cycling.

Microstructure may also influence the carbide precipitation and strengthening mechanism of chromium-molybdenum steels. In 2.25% Cr - 1% Mo steel, precipitation reactions are known to occur much more rapidly in bainite than in proeutectoid ferrite. In addition, the interaction solid-solution strengthening of 2.25% Cr - 1% Mo steel is found to be influenced by microstructure. Interaction solid-solution hardening in bainitic (normalised and

tempered) 2.25% Cr -1% Mo is due to chromium-carbon interactions, while it is due to molybdenum-carbon interactions in the proeutectoid ferrite of annealed steel [2].

3.2.3 EFFECTS OF HEAT TREATMENT

The use of tempering is also an important factor (figure 3.15) that influences the level of precipitation strengthening and solid-solution strengthening in chromium-molybdenum steel (figure 3.3). In a normalized molybdenum steel (figure 3.3A), the initial contribution from solid-solution strengthening is greater than that of the normalized and tempered steel. In the normalized and tempered molybdenum steels (figure 3.3B), the initial contribution from precipitation strengthening will be larger than that from the normalised steel. In addition the initial contribution from precipitation strengthening effect in the normalized and tempered steel will reach a maximum and begin to decline at an earlier stage due to the earlier incidence of overaging in tempered material. This is a potential consideration in applications requiring creep resistance over long time and at high temperatures (also refer fig 3.10 to fig 3.12).

3.2.4 EFFECTS OF COMPOSITIONS

Carbon

It is an austenizer, it forms interstitial solid solution in iron alloy system and improves both room and elevated temperature properties like increased yield strength, tensile strength and creep rupture value. It promotes dispersion strengthening through formation of carbides in the structure. It does not increase appreciable creep resistance at elevated temperatures above 540°C because carbides eventually become spheroidized at such temperature. For chromium containing steels, carbon content is usually kept 0.15% [2, 3].

Chromium

It is a ferrite stabilizer, and forms a very stable carbides, dispersed in the matrix helps in opposing high temperature deformation. In small amount (about 0.5 %) it is a carbide former and in large amounts (upto 9 % or more) it increases the resistance to scaling in air. It also forms a very stable passive film over the surface of the steel, to impart resistance to oxidation at elevated temperature. Though, chromium carbides i.e., $(FeCr)_3C$, $(CrFe)_3C_2$, $(CrFe)_7C_3$ are very stable at temperature below $600^{\circ}C$, but above this temperature these carbides rapidly coalesce and secondary carbides redissolve in the matrix, leading to decrease of creep rupture strength.

Chromium is most effective in strengthening molybdenum steels (0.5 % to 1.0% Mo) when it is used in amounts of 1 to 2.25 %. On increasing the chromium percentage above this limit, there results a decrease in creep strength of molybdenum steel, as shown in figure 3.14. Same trend is followed by tensile and yield strength of Cr - Mo steel, if Cr is increased above 2.25%, refer fig.3.13A and fig. 3.13B.

Molybdenum

It is a ferrite stabilizer, it helps in improving high temperature creep and rupture strength by stabilizing the chromium carbides and not allowing dispersed carbides to coalesce, It also helps to resist temper brittleness in alloy steels. Much greater creep strength can be obtained by increasing the molybdenum level to about 1% but at the expense of rupture ductility, addition of Cr can improve rupture ductility.

Addition of Mo above 4.5%, results in rapid tendency of steel to form intermetallic phases, particularly sigma phase, which limits section thickness and

weldability. The discovery that nitrogen slows down the formation of the intermetallic chromium-molybdenum sigma phase had led to the development of super-austenitics - 6Mo stainless steel, which has very good pitting resistance, corrosion resistance and crevice corrosion resistance [2, 3].

Upto 0.5% Mo it appears to be more effective in retarding pearlite and increasing bainitic formation [3]. Its addition to steel improves creep resistance and resistance to hydrogen damage from hydrogen rich process fluid. This enhancement in the properties results only from the formation of stable carbides.

Niobium and vanadium

They are added to improve elevated temperature properties. Vanadium is also added to some of the higher carbon steels to provide additional resistance to tempering and to retard the growth of carbides at service temperature. Niobium is sometimes added to these steel to increase their strength through the formation of stable carbides. Niobium and vanadium improve resistance to hydrogen attack, but may promote hot cracking.

Phosphorus and sulphur

They are considered undesirable because they reduce the elevated temperature ductility of steel. Sulphur results in hot shortness and phosphorus contributes to temper embrittlements.

Silicon

It increases the elevated temperature strength of steel. It also increases the resistance to scaling of the low chromium steel in air at elevated temperatures. Silicon is one factor in temper embrittlement.

3.3 WELDING METALLURGY

The Cr - Mo alloy steels are readily weldable. The air-hardening characteristics (refer fig. 3.16 & 3.17) of the Cr - Mo steels require that the welding procedures used should prevent cracking both in the weld metal and HAZ. In developing such procedures, the control of preheat, postweld heat treatment and electrode composition must be given proper consideration.

Where cracking is a problem, raising the preheat temperature (if it is low) and holding at that temperature for a proper length of time after welding has been completed, or until post weld heat treatment can be done will alleviate the problem. The preheat must be high enough to permit the escape of hydrogen that may be present. As the thickness and carbon & alloy content increases, the preheat temperatures must also increase to guard against cracking.

The filler metal, used for the welding of Cr - Mo steel, should have same nominal composition as base material, except for carbon content. However, the weld metal that are to be quenched and tempered or normalised & tempered and when efficiency of the joint required is 100%, matching carbon content will be necessary.

Austenitic stainless steel filler metals of 25% Cr - 20% Ni or 25% Cr - 12% Ni are often employed in minor repair welding work on the Cr-Mo steels, and are preferred for those application in which the weldment cannot be given postweld heat treatment. The weld metal in this case has a lower yield strength, but has excellent as welded ductility [9].

Austenitic weld metals are not satisfactory when the welds will be subjected to cyclic temperature in service. It is due to difference in coefficient of thermal expansion of ferrite base metal and austenitic weld metal.

The conditions in which chromium molybdenum steels are placed in service are :

- (a) without a post weld heat treatment,
- (b) with a sub-critical stress relief in the temperature range of 593 - 796°C, and
- (c) with an annealing heat treatment of the completed weldment [9].

Certain Cr - Mo steels can be put into service in the as - welded condition when proper preheating practices are employed and section size is not large.

The sub-critical post weld stress - relieving heat treatment is employed to reduce the hardness and residual stress level, and increase the ductility of the welded metal and the base metal HAZ.

Annealing of these steels consists of heating the weldment to a temperature in the range of 843-913°C, holding at that temperature for one hour per hour of thickness following by cooling at a maximum rate of 28°C per hour. This procedure results in a relatively soft ferrite structure throughout the weld metal, the heat affected zone and the base metal.

Whether post weld heat treatment should be applied when the weldment is still at the preheating temperature, or whether the weldment may be cooled to ambient temperature before it is given such treatment, will depend on welding restraint stress, chemical composition of the base and weld metal and preheats practice used.

If it is not practical to heat treat from the preheat temperature, raise the weldment temperature from the preheat temperature to at least 427°C and hold this temperature for 2 or 3 minutes per inch of thickness before cooling to room temperature. This will prevent cracking until the weldment can be heat treated.

This low temperature stress relief should not however, be considered as a substitute for proper postweld heat treatment.

3.4 DEGRADATION OF PROPERTIES DUE TO LONG TERM ELEVATED TEMPERATURE EXPOSURE

When low alloy steels are exposed to elevated temperature during service, their properties deteriorate due to change in microstructure and diffusion of impurities such as P, Sn, As and Sb to the grain boundaries. Addition of Mo upto 0.7% is known to reduce temper-embrittlement susceptibility of 2.25Cr - 1Mo type steel. Molybdenum suppresses embrittlement by scavenging phosphorus through the formation of a Mo-P compound and thus decrease phosphorus segregation to the grain boundaries, But, the fact that molybdenum content in the matrix decreases, due to the formation of molybdenum carbides (M_2C or M_6C) during tempering or aging, significantly enhances embrittlement susceptibility of 2-25 Cr-Mo steel [6].

Temper embrittlement results in shift of the charpy V-notch impact energy transition curve to a slightly high temperature. Since the operating conditions of presence vessels made of 2 1/2 Cr - 1Mo. C in the temperature range of 370 - 470°C, temper embrittled weld deposits will perform satisfactorily at operating temperatures. The only concern would be during shut-down or startup periods. During such periods brittle behavior of temper embrittled material can be avoided by the simple expedient of heating the pressure vessel to above say 100°C, before applying pressure to the vessel [5].

**LITERATURE REVIEW - II
(HYDROGEN INDUCED CRACKING)**

4.1 INTRODUCTION

The damaging effects of hydrogen in metals are known since about a century. Embrittlement by hydrogen damage manifests itself as a decrease in tensile ductility, a reduction in notch toughness and delay failure by fracture under static loading. In chemical industries, where high concentration of hydrogen is common, these type of cracks often experienced in these industries [10].

Hydrogen induced cracking also may occur in steel if the steel contains absorbed hydrogen and is cooled too rapidly after prolonged exposure to elevated temperature. The excess hydrogen then cannot escape during cooling and produces cracking.

In quenched and tempered steels, hydrogen cracking usually follows prior austenite grain boundaries.

4.2 HYDROGEN EMBRITTLEMENT

The solubility of hydrogen in ferrite is virtually negligible, it increases with increase in temperature. At the temperature of ferrite to gamma transformation, the solubility increases abruptly and continues to rise. There is a dip in solubility of hydrogen in delta iron, but again it increases with temperature upto melting point. The amount of hydrogen dissolved at a given temperature is proportional to the square root of the hydrogen gas pressure outside the steel and is given by Sievert's law [10],

$$C = K \cdot (P_{H_2})^{1/2}$$

When steel is cooled from elevated temperature, there is a sharp decrease in the solubility of hydrogen and thus, steel becomes supersaturated. Hydrogen dissolved in the lattice by either of these methods will diffuse out of the metal lattice and recombine to molecular hydrogen. This can occur either in the atmosphere near the surface of the steel or within the steel in discontinuities, grain boundaries, around the inclusion or in voids. In this way, pressure of molecular hydrogen builds up in these discontinuities and steel becomes weaker.

Diffusivities of hydrogen in BCC is many order of magnitude more than that in FCC. Thus, hydrogen embrittlement is expected to be more for ferrite than in austenite. Additionally, effect is compounded by lower ductility and high notch sensitivity of alpha as compared to gamma iron [10].

Hydrogen embrittlement is sensitive to strain rate and temperature. The embrittlement is enhanced by low strain rate and moderate temperature. At very high strain rate, hydrogen is not transported to voids at a sufficient rate to keep up its pressure. Increasing temperature generally retards cracking by homogenizing the hydrogen and thus avoid high local concentration [11].

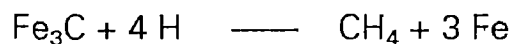
The position of cracked initiation is observed to vary with notch severity. Sharply notched specimens crack slightly below the notch bottom and in case of less sharp notches more deeply. This is in agreement with the concept that the position of maximum triaxial stresses moves into the specimen as the notch severity is decreased.

If heat of solution, ΔH is small or zero, the solubility of hydrogen in the structure will be large and reduction of cohesive strength will be small. This is in accordance with the difficulty of producing hydrogen embrittlement in stable austenitic steel [10].

If heat of solution, ΔH is positive, the solubility of hydrogen in the structure will be small and thus, reduction of cohesive strength will be more, thus favours, more hydrogen embrittlement (HE).

The mechanism of HIC formation is still being investigated. An early hypothesis, involving the build up of hydrogen gas pressure in voids, is now generally discredited. Currently, the most widely accepted model involves the presence of pre-existing defect sites in the material - small cracks or discontinuities caused by minor phase particles or inclusions. In the presence of existing stress, these sites may develop high local areas of biaxial and triaxial tensile stress. Hydrogen diffuses preferentially to these sites of dilated lattice structure.

As the local hydrogen concentration increases, the cohesive energy and stress of the lattice decrease. When cohesive energy falls below the local intensified stress level, fracture occurs spontaneously. Hydrogen reduces the work function of cementite-ferrite bonds and thus provide easier path for crack propagation. Reaction is as follows,



Small amount of hydrogen is needed to form thin layer of methane and to reduce work function to zero. Carbide formation often occur preferentially at grain boundaries, and as grain boundaries are likely sinks for hydrogen during cooling, this reaction appears to provide a feasible explanation for the grain boundaries rupture of cold cracking [12].

4.3 FACTORS AFFECTING HYDROGEN INDUCED CRACKING

HIC basically depends on three mutual interactive factors, they are :-

- 1) Presence of hydrogen (even very small amount i.e. parts per million).
- 2) High residual stresses.
- 3) A susceptible microstructure.

4.3.1 EFFECTS OF HYDROGEN

As we have already discussed that solubility of hydrogen in austenite is much more than in ferrite, due to which hydrogen solubility decrease when austenite transform to ferrite. As hydrogen has got high diffusivity in alpha iron, this helps to accommodate differences in solubility associated with the austenite - ferrite ($\gamma \rightarrow \alpha$) transformation. Thus, as the transformation proceeds austenite become progressively more enriched in hydrogen. As austenite to martensite transformation occurs at the lower temperatures and originates from the most hydrogen enriched austenite, microstructure obtained become sensitive to HIC. Twinned martensite is more dangerous than lath martensite, this could be due to low M_s temperature for twinned martensite [12].

4.3.2 ROLE OF STRESS

A certain minimum value of stress and certain minimum concentration of hydrogen is required for cracking to occur due to hydrogen embrittlement. If concentration of hydrogen is decreased, more stress will be required to initiate delayed cracking. Cracks of this type usually occur in the region of high triaxial stresses. The position of crack initiation is observed to vary with notch severity, this is due to change in the position of high triaxial stresses with change in notch severity [12].

4.3.3 ROLE OF MICROSTRUCTURE

Microstructure plays an important role in assisting / retarding HIC. Increase in grain size effectively decreased the transformation temperature so than in steel having high carbon equivalent, volume portion of the lower temperature transformation products such as martensite, bainite or widmanstatten side plates increases. High dislocation densities associated with these products, together with fine carbide particle hardening, results in hard and low ductile matrix [12, 13].

Another effect of larger prior austenite grain size is to increase the amount of segregation at boundaries.

4.4 HYDROGEN CRACKING IN WELDMENTS

HIC has been correlated both with material hardness and strength, and with specific microstructure. High strength steels are more susceptible to HIC than low strength steel. Steels that transforms martensitically are particularly susceptible, especially the high carbon alloys with twinned martensite structures. The form of the ferrite produced during transformation on cooling from the austenite phase field is also critical, with accicular ferrite resulting in improved properties compared with grain-boundary ferrite, polygonal ferrite or widmanstatten ferrite. Accicular ferrite is often nucleated on minor phase particles, such as specific oxides or borides. Acknowledgment of the beneficial effect of certain oxides in providing sites for accicular ferrite nucleation in modern steels is in sharp contrast to steel design of earlier decades, when elimination of oxygen to the greatest extent possible was considered essential to the development of optimal fracture behaviour.

A useful concept for understanding the susceptibility of carbon and alloy steels to hydrogen induced cracking is the carbon equivalent (CE), an empirical

relationship that attempts to reduce the number significant compositional variables affecting the weldability of steels into a single quantity [13].

$$CE = \%C + \frac{\%Mn}{6} + \frac{\%Cr + \%Mo + \%V}{5} + \frac{\%Si + \%Ni + \%Cu}{15}$$

From a metallurgical perspective, the carbon equivalent can be related to the development of hydrogen sensitive microstructures. That is, as the carbon equivalent increases, microstructures are evolved during cooling through the transformation temperature range that are increasingly more susceptible to hydrogen induced cracking. At high carbon equivalent values, martensitic structures can be expected.

When carbon equivalent exceeds 0.35 %, preheating is recommended to minimise susceptibility to hydrogen cracking. At higher level of carbon equivalent, both preheat and postheat may be required. Thicker section often require preheating because of the greater heat-sinking capability of a thick section, for which a given set of welding parameters will produce a faster cooling rate.

Postheating has its own advantage in resisting HIC. It reduces the residual stresses present in the as welded structure. Microstructural modification such as tempering can also occur, producing a microstructure less susceptible to HIC [13].

Finally, the higher temperature may allow hydrogen to diffuse into the bulk of the structure or even to the surface, where it may recombine and exit as gas. In either case, the level of hydrogen concentration may be reduced below that required to initiate cracks.

4.5 FEATURE OF HYDROGEN INDUCED CRACKING IN SEM

Fractures in Q & T high strength steel by stress corrosion cracking (SCC) and hydrogen embrittlement (HE) are intergranular when the stress intensity at the tip of the propagating crack is low. The fracture path is along the prior austenitic grain boundaries, and the fine detail revealed on the grain facets can be related, either to plasticity effects associated with the fracturing processes or to corrosion effects associated with certain aqueous environment, where they are present.

The grain facets show some evidence of ductility but it is usually confined to only narrow region of the grain boundaries. Fracture initiated by diffusion of hydrogen into the steel, and mainly starts from sub-surface where triaxial stresses are maximum. Fine tear ridges (hair line indication) is common on separated grains facets is the unique feature of HE. Tear ridges formed when cracks that were initiated as a result of hydrogen charging grew together. At higher magnification, evidence of limited amount of deformability is observed in the form of ridges or dimples on the separated grain facets. Transgranular cleavage may succeed intergranular separation as the crack lengthens, because of increasing stress intensity. Intergranular features such as those cause by HE, SSC, brittle grain boundaries show no evidence of microvoid coalescence, they have a "rock - candy" appearance.

Features of cracking caused due to SCC & HE resembles each other. However, fracture associated with SCC are distinguished by pronounced secondary cracking or deep crevice and the fracture shows great amount of corrosion product at the origin or in slow growth region than in the rapid fracture (dimpled) region.

**FAILURE ANALYSIS OF WELD SEAM
- A CASE STUDY**

5.1 FAILURE ANALYSIS REPORT

The AMMONIA SYNTHESIS CONVERTOR which was made of 2.25% Cr - 1% Mo steel was found cracked (Fig. 5.1) from one of its circumferential weld seam after six months of service. On inspection, it was found that 20 distinct cracks were present on the weld seam, these cracks were localized in the weld segment of 1.5 metre. This multilayer pressure vessel was made of three layers of SA 387 Gr22 Class 2 plates, each 48.5 mm thick. Operating temperature and pressure are 375-420°C and 130-140 Kg/cm² respectively. The reactor was build in multi wall technique with three walls. The welds for the single wall and the manufacturing of the prefabricated components was realised in workshop, while the circumferential welds to connect the prefabricated components together was performed on site. Two weld seams, i.e., seam no. 3 and seam no. 6 were welded at site. After 6 months of service seam no. 6 was found cracked. Cracks were observed only in the localised region of 1.5 metre, other portion of the seam did not show any sign of cracks.

5.1.1 INTRODUCTION OF THE EQUIPMENT

The Ammonia Synthesis Convertor, in which nitrogen and hydrogen combines over iron catalyist to give ammonia and heat is shown in fig. 5.1 and fig.5.2. Reaction is as follows:-



Operating conditions (Refer table 5.1)

Pressure — 130 - 140 Kg/cm²

Temperature— 375 - 420 °C

5.1.2 WELDING PROCEDURE FOLLOWED

— preheating temperature 225° C is maintained before welding.

— Maximum interpass temperature 250° C

— Electrode used AWS SFA 5.5 :E 9018

Yield strength — 5400 – 6700 Kg/cm²

Tensile strength — 6250 – 7500 Kg/cm²

Percentage elongation — 17 – 25%

— Electrodes baked to 325 - 375° C for 2 hrs.

— After completion of welding, intermediate stress relieving is done before the preheat temperature falls to 100° C (Refer fig 5.3).

— Perform Magnetic particle test, Dye penetrant test, Ultrasonic test, Radiography test.

— Carry out PWHT (Refer fig 5.4).

5.2 HISTORY OF EQUIPMENT FAILED (AMMONIA SYNTHESIS CONVERTOR)

To find the possibility of any operation flaws, available records on operating parameters of AMMONIA SYNTHESIS CONVERTOR from its initial start up, were examined. It was found that operating condition have never exceeded the limits.

According to the nelson curve as shown in Fig. 5.34A and operating

conditions, shown in Fig. 5.2 and Table 5.1, it is clear that for a operating hydrogen partial pressure of 8.962 MPa, the safe limit upto which operating temperature can go without causing surface decarburization (or hydrogen attack) in 2.25% Cr - 1% Mo steel is 525°C.

5.3 PRELIMINARY EXAMINATION OF THE WELD SEAM

VISUAL INSPECTION

After removal of the external insulation, cracks were found on the external reactor surface, transverse and longitudinal cracking with respect to circumferential weld was observed and was found completely contained within the weld metal.

NON - DESTRUCTIVE TESTING

Dye-Penetration test

DP test was performed to have a quick look of the surface condition, and it was found that in the one and a half metre length of weld joint, nineteen distinct cracks were observed. Transverse, as well as longitudinal cracks were observed in the weld metal. Photograph is shown in figure 5.32 to 5.38.

Magnetic particle test

Result of this test is same as that of DP test.

Ultrasonic Hardness Test (From outside the vessel)

To record the hardness value of various points on the cracked weld seam we marked the seam as shown in the figure 5.5 . We found that hardness value was found exceeding the limit of 250 HV (refer table 5.2) in the region from point number 8 to 12 where cracks were observed.

According to the Haldor Topsoe A/s specification, hardness value in material have to be kept below 250 HV to avoid the risk of potential damage due to hydrogen induced cracking.

Ultrasonic Hardness Test (From inside the vessel)

Hardness test was performed on the weld seam from inside the vessel also, so as to compare it from hardness value obtained from outside the vessel. Results obtained from these test showed that hardness value is well within the safe limit of 250 VHN refer table 5.3.

5.4 SAMPLES FOR FURTHER ANALYSIS

For further study of this failure, three samples from three different locations of weld seam were taken, refer fig 5.6 . Sample which was named 'A1' is taken from that portion of the weld seam, where cracks were observed. Sample which was named 'B1' is taken from that portion of the weld seam, which was adjacent to the 'A1'. Sample which was named 'C1' , is taken from the crack free zone of weld seam, which was just opposite to 'A1' zone.

5.4.1 WELD SEAM ZONE A₁ (Refer fig 5.6)

It is this zone, where cracks were observed in both longitudinal and transverse direction, with respect to circumferential weld seam. Cracks were found completely contained within the weld metal. These cracks appeared after six months of service in hydrogen atmosphere. Chemical analysis, hardness test, metallography of the fractured zone and fractography of the fractured surface were taken, to study the crack behaviour.

CHEMICAL ANALYSIS (REFER TABLE 5.7)

Chemical analysis was done and it was found that was exactly as per the

requirement of the standard specification of A387 Gr. 22 Cl. 2 steel (Refer table 5.10).

HARDNESS TEST (REFER TABLE 5.1 & 5.2)

Hardness values were recorded throughout the defective seam, it showed abnormal readings only in the zone, 8 to 12 (where cracks were observed) as marked in the fig 5.5 . These abnormal readings in the selected area (or zone), could be due to non-uniform post weld heat treatment.

METALLOGRAPHY

Microstructure

To study the microstructure of A₁ zone, some photograph of unetched and etched surface were taken. It was found that crack was completely contained within the weld metal. Some branching of cracks were observed (fig 5.7 to fig 5.10) and the cracks were found intergranular, refer fig 5.8 to fig 5.10. Crack was found propagating along the prior austenite grain boundaries, refer fig 5.11. Microporosities were also observed in the microstructure, refer fig 5.7 to 5.9 & also fig 5.12. .Microstructure of weld metal and HAZ shows some sign of columnar grains, refer fig 5.13 & fig 5.14 , but parent metal was found free from any directionality, refer fig 5.16 . Some amount of coarsening of carbides were observed in the parent metal, refer fig 5.16.

FRACTOGRAPHY

Zone A₁ is which cracks were observed, was cut in such a way so as to expose the fractured surface for SEM fractographic examination to determine the cracking mode. On exposing the fractured surface, three layers were observed. These layers were not perfectly visible, because of oxide film over the fractured surface. Solution of ammonia citrate and ammonium oxalate was tried to remove

the oxide layer. After removing the oxide layer, three layers were found visible distinctly.

First layer, where cracks would have initiated, has a shining appearance, which gives an indication of brittle zone.

Second layer, has dull and fibrous appearance this confirm of ductile layer, this shows a ductile layer.

Third layer, shows the area of over load stress.

Ultrasonically cleaned surface was then examined under SEM, fractographs obtained are enclosed from fig. 5.17 to fig. 5.26. It is clear from the fractographs that it is a case of hydrogen embrittlement which has resulted in inter-granular cracking (refer fig. 5.17, 5.21 & 5.22). Fine tear ridges typical of hydrogen induced cracking is also evident in fig. 5.17, 5.19, 5.24 & 5.26.

Extent of deformability varies from very poor deformed (refer fig. 5.21 & 5.22) to very heavy deformed regions (refer fig. 5.18 & 5.23). Transgranular cleavages are also observed in some of the regions (fig. 5.19 & 5.21), this is due to increase in stress intensity as crack proceeds (intergranularly).

Heterogeneity in structure is also frequently observed. Cast features such as columnar grains (refer fig. 5.13 & 5.14), multipass weld zones are all visible in different locations. Cracks have also propagated along columnar grains (refer fig.5.22). All this indicates insufficient post weld treatment which seems to be the ultimate cause of failure.

5.4.2 WELD SEAM ZONE B₁

In this zone, which is adjacent to the cracked zone A1, two types of samples were taken, one longitudinal and other transverse with respect to

circumferential weld, so as to compare the mechanical properties in two orthogonal directions. Transverse samples were marked as B(T) and longitudinal as B(L).

CHEMICAL ANALYSIS (REFER TABLE 5.7)

Chemical analysis was done and it was found that was exactly as per the requirement of the standard specification of A387 Gr. 22 Cl. 2 steel (Refer fig.5.10).

HARDNESS TEST

Vicker's hardness test was conducted on both types of samples i.e. longitudinal and transverse of B₁ zone, with the help of 30 Kg load which is applied for 25 seconds, so that the diamond impression can be obtained on the surface of the sample. Both the diagonals were recorded and average value is taken for calculating hardness value in Kg/mm². Hardness values observed were found high, for longitudinal samples hardness values were found varying from 203 to 313 (table 5.4), exceeding the limit of 250 HV imposed, to avoid hydrogen embrittlement. Results of hardness test of transverse samples showed alarmingly high values, as shown in table 5.4 . There was a vast difference in the hardness values in longitudinal and transverse direction. This shows that the material was anisotropic, which could be the result of non-uniform post weld heat treatment.

TOUGHNESS TEST

Charpy standard samples (as shown in fig 5.27) were tested for both, longitudinal and transverse samples to record the energy absorbed to break the specimens. It was found that transverse samples absorbed more energy than longitudinal samples before these fail, refer table 5.5. Results of this test confirms the results of hardness test i.e., non - uniform post weld heat treatment.

TENSILE TEST (REFER FIG 5.28)

Tensile test also confirms the inhomogeneity in the structure. Longitudinal samples were found to have UTS in the range of 5000 Kg/cm² whereas transverse sample showed in the range of 9800 Kg /cm², refer table 5.6. As per ASTM standards, tensile strength of A387 Gr22 Cl. 2 should have tensile strength in the range of 5150 to 6900 Kg/cm², refer Table 5.9. Ductility in longitudinal samples where found more refer the graph shown in fig 5.32 A & fig 5.33 B.

5.4.3 WELD SEAM ZONE C₁

CHEMICAL ANALYSIS (REFER TABLE 5.7)

Chemical analysis was done and it was found that was exactly as per the requirement of the standard specification of A387 Gr. 22 Cl. 2 steel (Refer Table 5.10).

METALLOGRAPHY

The microstructure of WM is perfectly regular and is as per ASTM standards for A387 Gr. 22 Class 2. Microstructure resembles quenched and tempered structure with some sign of carbide precipitation. Retained austenite were also observed in the microstructure. Some amount of carbide precipitation were also observed along the grain boundaries, but their amount was not alarming refer fig. 5.29 to 5.31.

HARDNESS TEST

Vicker's hardness test was conducted with the help of 30 Kg load which is applied for 25 seconds, so that the diamond impression can be obtained on the surface of the sample. Both the diagonals were recorded and average value is taken for calculating hardness value in Kg/mm². Result of this zone were acceptable refer table 5.8.

RESULTS AND DISCUSSIONS

1. Coarse carbides were observed in the microstructure and some of them have preferentially precipitated along grain boundaries (Fig. 5.29). As grain boundaries are likely sink for hydrogen, these carbides get attacked by hydrogen and results in the formation of thin layer of methane which reduces the work of adhesion between the grains to-zero. This makes the steel weaker along the grain boundaries.

This problem could have been very easily avoided, if proper post-weld-heat treatment would have been done. Though the cycle of PWHT followed is exactly matching the requirement for A387 Gr. 22 steel, but has not given the intended results because number of thermocouples used were only six, with this small number we cannot ensure homogeneous temperature throughout the seam during PWHT. Our purpose is to stress relieve the entire weld seam, which is seven metre long and 150 mm thick, and so we should use atleast eight thermocouples from inside the vessel, and eight thermocouples form outside, to have a better control on rise and fall of temperature during PWHT.

2. Coarse prior austentic grains were observed (Fig. 5.10) near the area where cracks were found. Cracks were found propagating along these coarse prior austentic grain. Increase in grain size decreases the transformation temperature so that in steel having high carbon equivalent, volume fraction of the lower temperature transformation product such as martensite or bainite increases. High dislocation densities associated with these structures result in hard and less ductile matrix.

Another effect of larger prior austenite grains, is to increase the amount of

segregation at grain boundaries. And thus, makes the steel weaker along the grain boundaries.

Coarse prior austenitic grains in some region of weld seam, gives an indication of improper post weld heat treatment (as discussed in point number 1 above). It is not that the procedure followed for PWHT is faulty, but it is the technique of PWHT. No. of thermocouples used to keep a track of temperature (rise or fall) during PWHT were less in number, which has resulted in inhomogeneous heat treatment along the weld.

3. Columnar grains were observed (Refer Fig. 5.13, 5.14) in the microstructure of HAZ and weld metal of A₁ zone (zone in which cracks were detected). Columnar grains gave the directionality to the weld metal, which is evident in the results of tensile and toughness test (refer table 5.5 & 5.6) weld metal was found to have better mechanical properties in transverse direction as compared to longitudinal direction.

Abrupt change in properties acts as a notch, which initiates cold cracking.

Columnar grain of A₁ zone and equiaxed grain of C₁ zone gives an indication of non uniform PWHT. On further investigation it was found that thermocouples used to monitor the temperature during stress-relieving cycle were insufficient in numbers.

When insufficient numbers of thermo couples are used, the problem of over-heating or under-heating some region is very common especially if the seam length is as big as 7 meters and 150 mm thick. It is necessary to use at least one thermocouple for each heating coil, which is not used here, which has resulted in cracking.

4. Some amount of porosity was also observed (Fig. 5.7 & 5.8). On cooling, when hydrogen solubility decreases. Hydrogen dissolve in the lattice, diffuse out of the metal lattice and accumulate at discontinuities like grain boundaries or voids) where it form its molecule. Due to this, pressure in the voids builds up and the steel become weaker.

Porosity can easily be avoided by using properly baked electrodes, so that moisture absorbed by electrodes during storage, can be removed.

5. The possibility of high temperature hydrogen attach phenomenon, has been ruled out, as there is no evidence which supports decarburization, (refer fig. 5.7 to 5.12). Moreover, operating parameters have never exceeded the limits.

6. To improve the resistance of steel against hydrogen embrittlement, we suggest inter-critical quenching between normal quenching and tempering.

The reason why resistance improves against hydrogen embrittlement is because of restricted amount of segregation of impurities at austenite grain boundaries, small amount of ferrite in the structure, austenite grain refined and fine, and homogenous carbide are distributed over the structure.

Intercritical quenching i.e., quenching from ($A_{c3} - X^{\circ}C$) results in optimum amount of ferrite in the microstructure. Stress raisers of the martensite may be relaxed since there is ferrite around martensite. Since hydrogen can be absorbed by the ferrite as hydrogen trap and the movement of hydrogen is blocked, the concentration of hydrogen at grain boundaries is restrained and the fracture strength is increased [11].

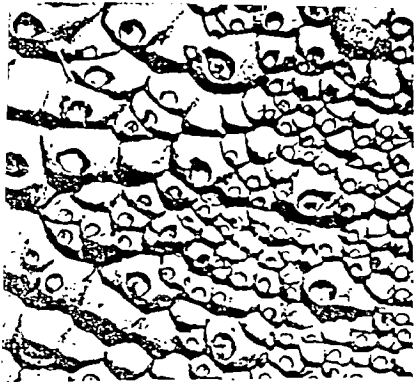


Fig.2.1 TEM fractograph, at 40,000 \times , of a carbon replica of the surface of a ductile-brittle fracture, showing dimpled pattern typical in overstress fractures of ductile metals and alloys

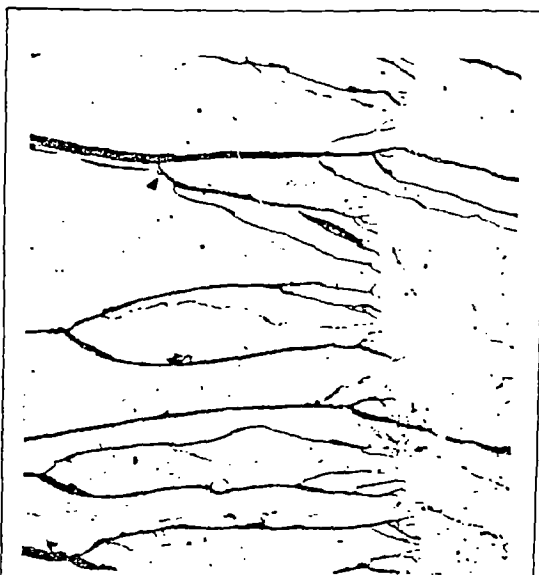


Fig.2.2 Fractograph, at 16,000 \times , of a fracture surface in a zinc specimen, showing a cleavage facet containing river marks generated by a subgrain boundary



Fig.2.3 TEM fractograph, at 6000 \times , of a plastic-carbon replica of the surface of a brittle fracture in steel that resulted from intergranular stress-corrosion cracking, showing a pattern of small angle tilts and an absence of deformation

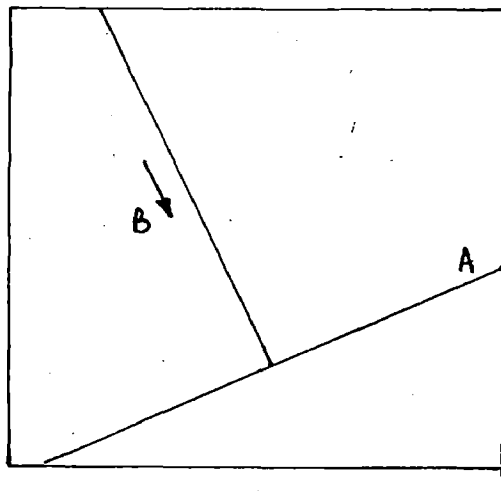


FIG 2.4 Schematic illustration of the sequencing of cracking by the T-JUNCTION procedure where crack A precedes and arrests fracture B

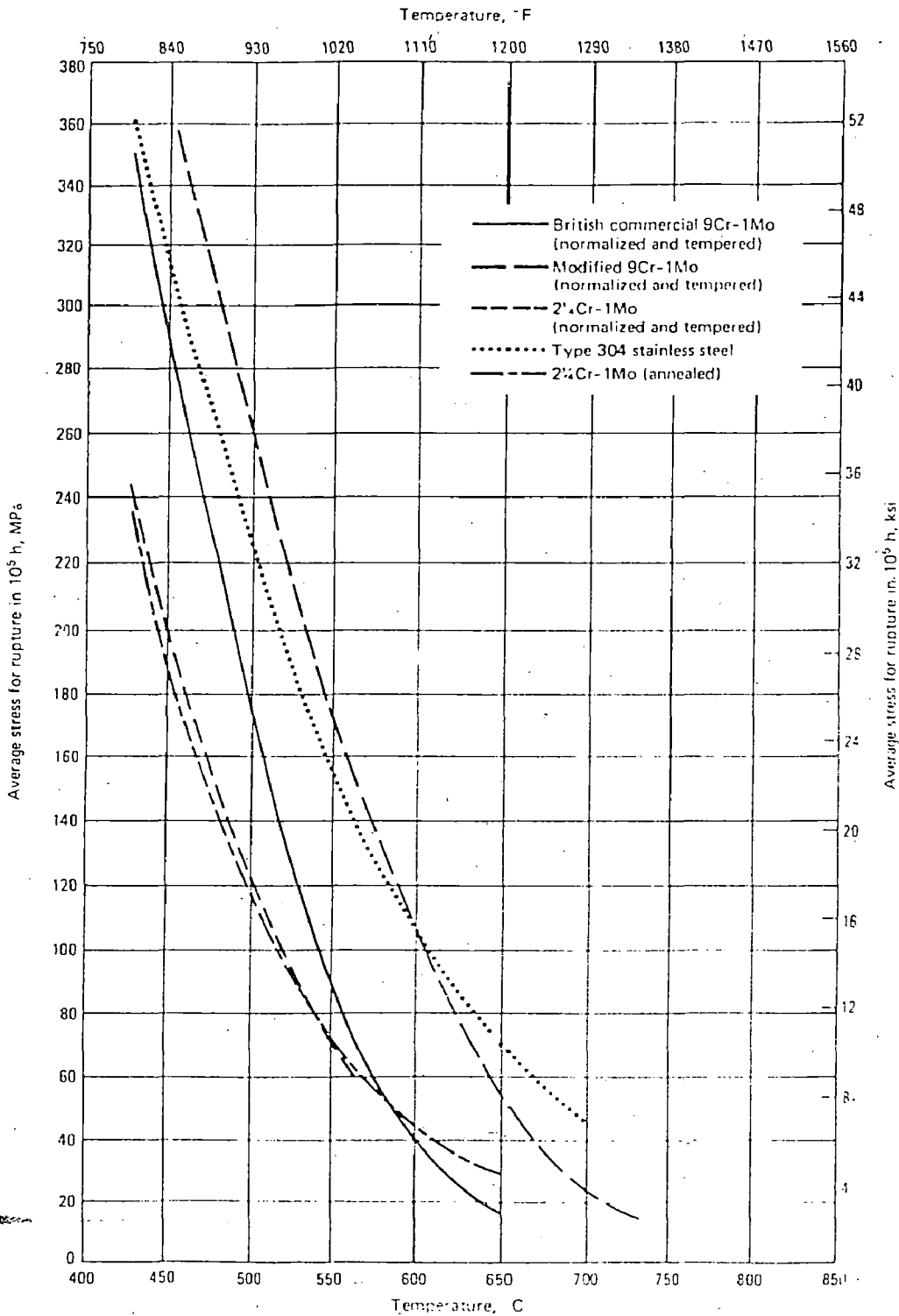


Fig. 3-1 Variation of 10^5 h creep-rupture strength as a function of temperature for 2 1/4Cr-1Mo steel, standard 9Cr-1Mo, modified 9Cr-1Mo, and 304 stainless steel. Source: Ref 7

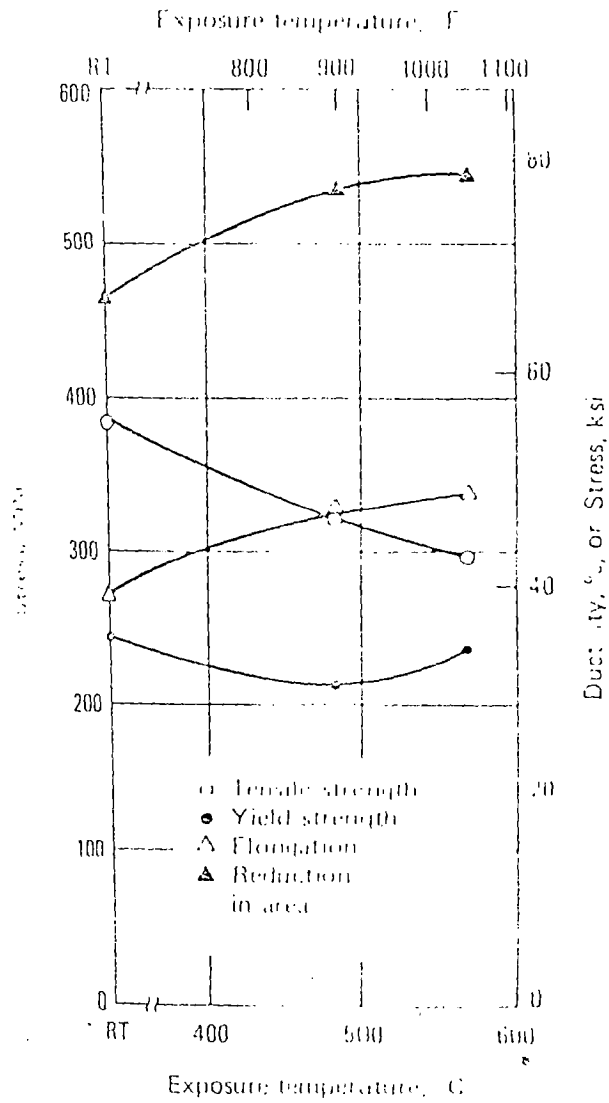


Fig. 32 Effect of elevated temperature exposure on the room temperature tensile properties of normalized 0.17% C steel after exposure (without stress) to indicated temperature for 83 000 h.

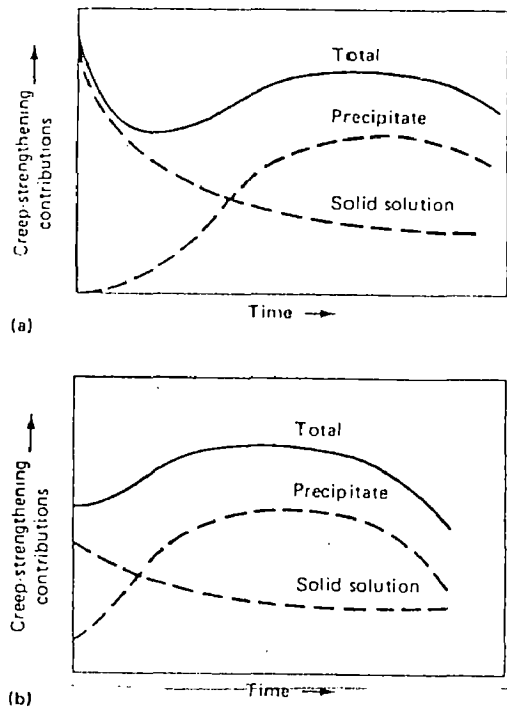


Fig. 3.3 Schematic of changes in creep strengthening contributions at 550 °C (1020 °F) in (a) normalized molybdenum steel and (b) normalized and tempered molybdenum steel. Source: Ref 57

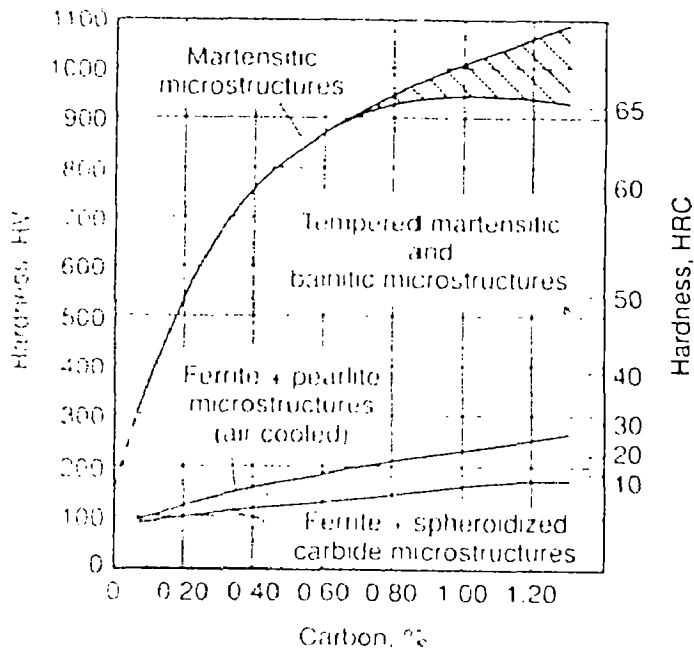


Fig. 3.4 Hardness as a function of carbon content for various microstructures in steels. Cross-hatched area shows effect of retained austenite. Source: Ref 1

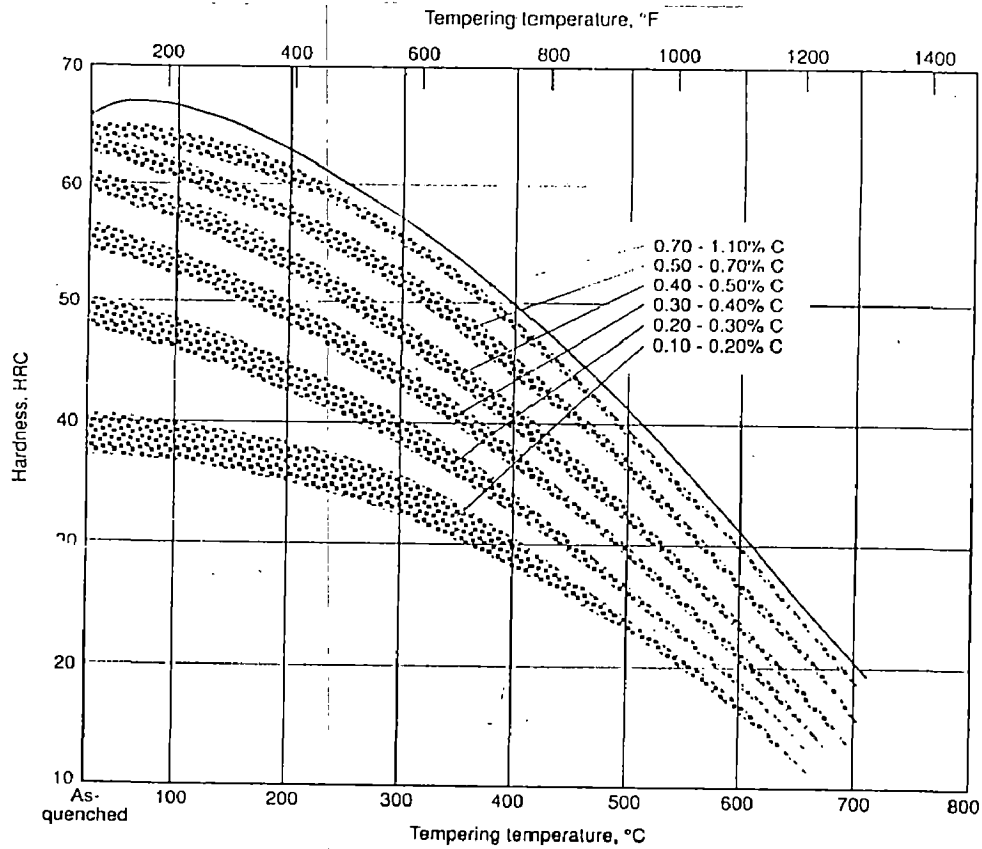


Fig. 35 Decrease in hardness with increasing tempering temperature for steels of various carbon contents. Source: Ref 61

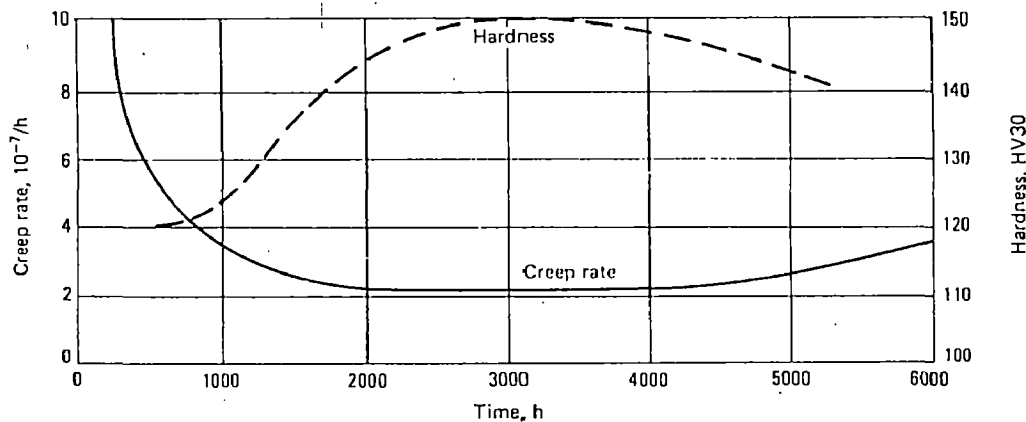
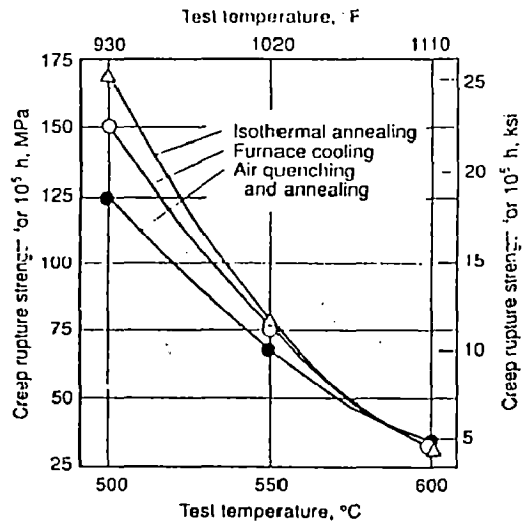


Fig. 36 Relationship between change in creep rate and change in room-temperature hardness during creep of normalized 1% Mo steel tested at 123 MPa (17.8 ksi) at 550 °C (1020 °F). Under these test conditions, secondary creep coincided with maximum precipitation hardening. Source: Ref 57



3.7

Fig. 3.7 Influence of heat treatment on 10⁵-h creep rupture strength of 2 1/4Cr-1Mo steel.

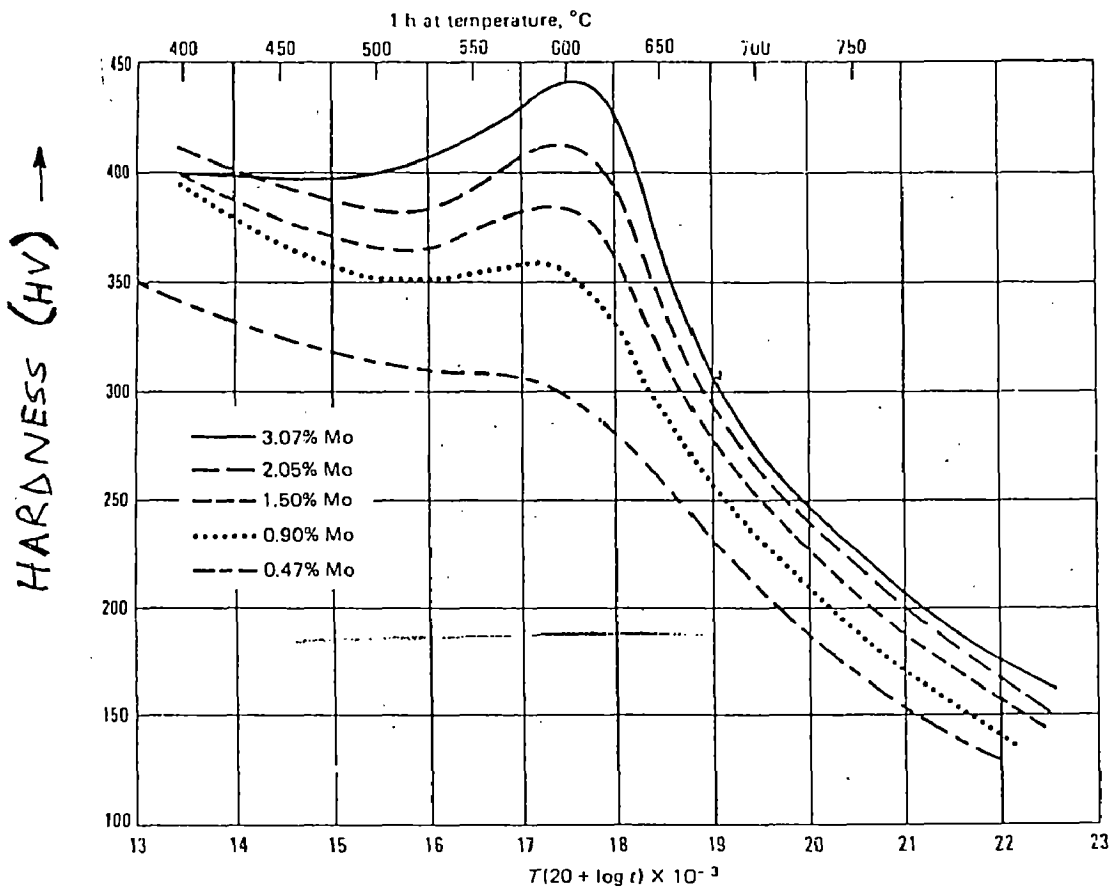
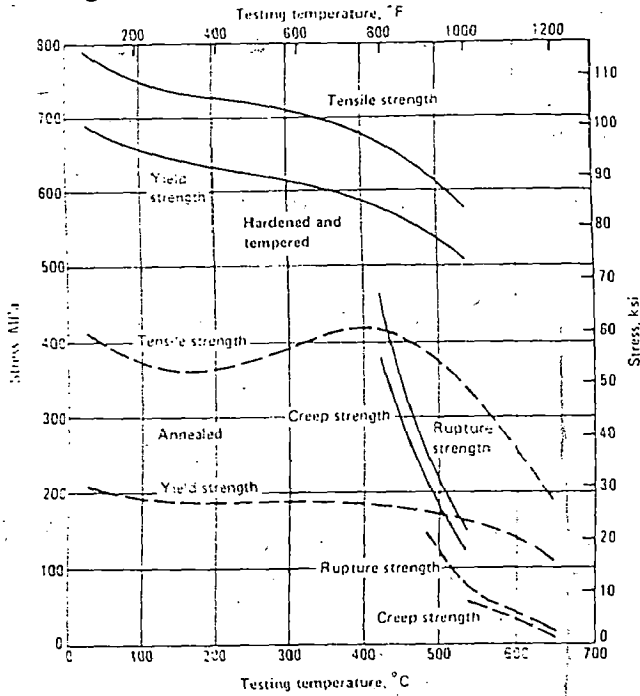


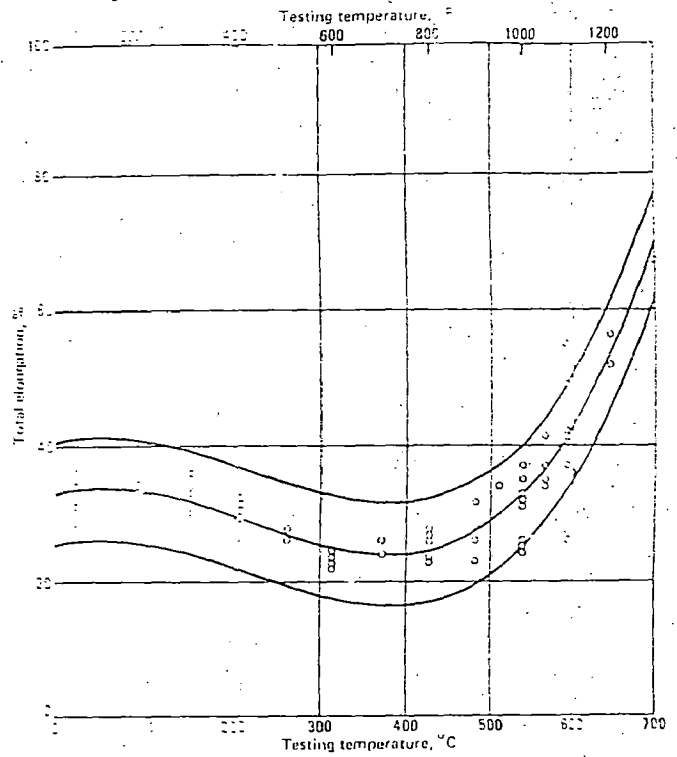
FIG 3-8 Retardation of softening and secondary hardening during tempering of steels with various molybdenum contents. Source: Ref 61

Fig. 3-10 Effect of test temperature on strength of 2 1/4Cr-1Mo steel



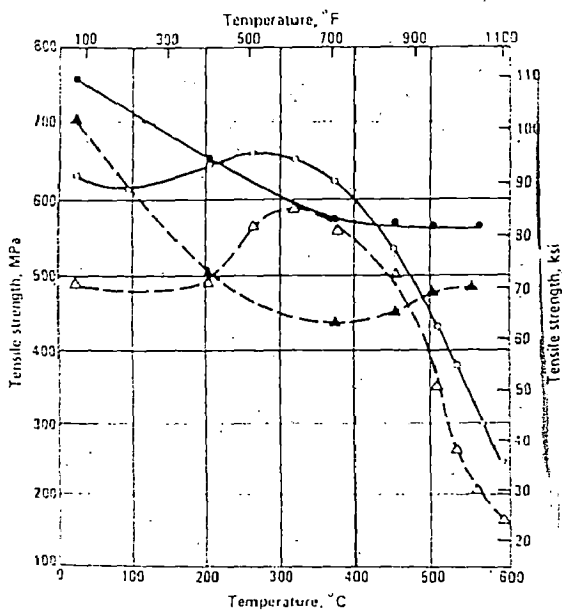
Effect of test temperature on tensile strength, yield strength, creep strength (for creep rate of $0.1 \mu\text{m/m}^2\text{h}$) and stress to rupture (for life of 100 000 h) of annealed specimens (dashed lines) and hardened and tempered specimens (solid lines) of 2 1/4Cr-1Mo steel

Fig. 3-11 Effect of test temperature on ductility

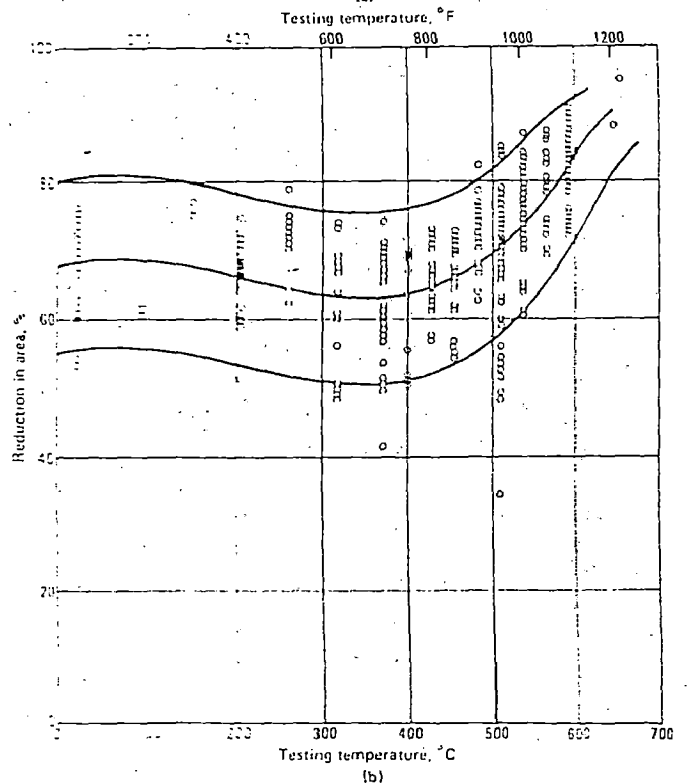


(a) Elongation to failure and (b) reduction in area, for annealed specimens of 2 1/4Cr-1Mo steel tested at the indicated temperatures

Fig. 3-12 Effect of strain rate on elevated temperature tensile strength of 2 1/4Cr-1Mo steel



annealed specimens (triangle symbols) and normalized and tempered (circles) specimens of 2 1/4Cr-1Mo steel were tested at strain rates of $2.67 \mu\text{m/m}^2\text{s}$ (open symbols) and $144 \mu\text{m/m}^2\text{s}$ (filled symbols) at the indicated temperatures



(a) Elongation to failure and (b) reduction in area, for annealed specimens of 2 1/4Cr-1Mo steel tested at the indicated temperatures

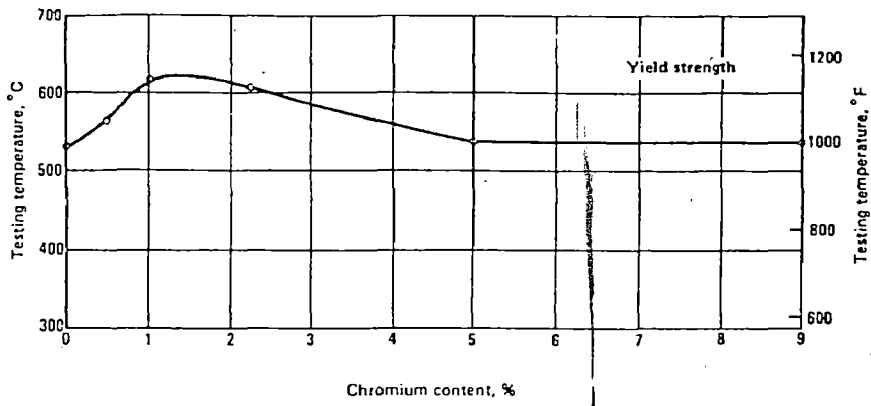


FIG 313A

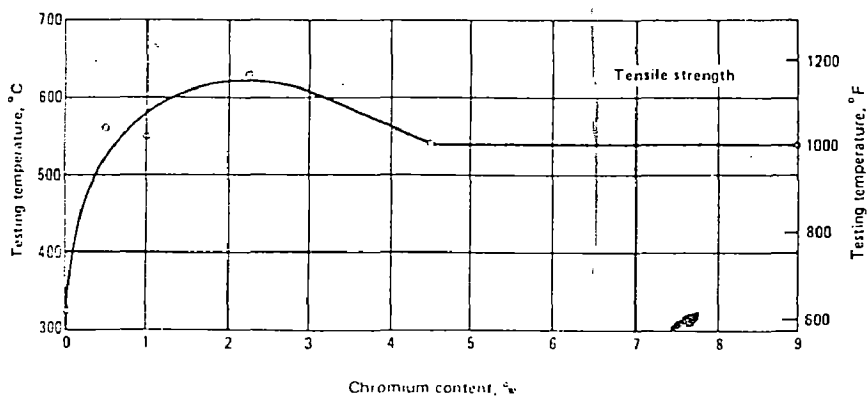


Fig. Effect of chromium content on strength. Test temperature required to reduce tensile strength and yield strength to 60% of their room-temperature values for chromium-molybdenum steels containing 0.5 to 1.0% Mo and the indicated amount of chromium

FIG 313 B

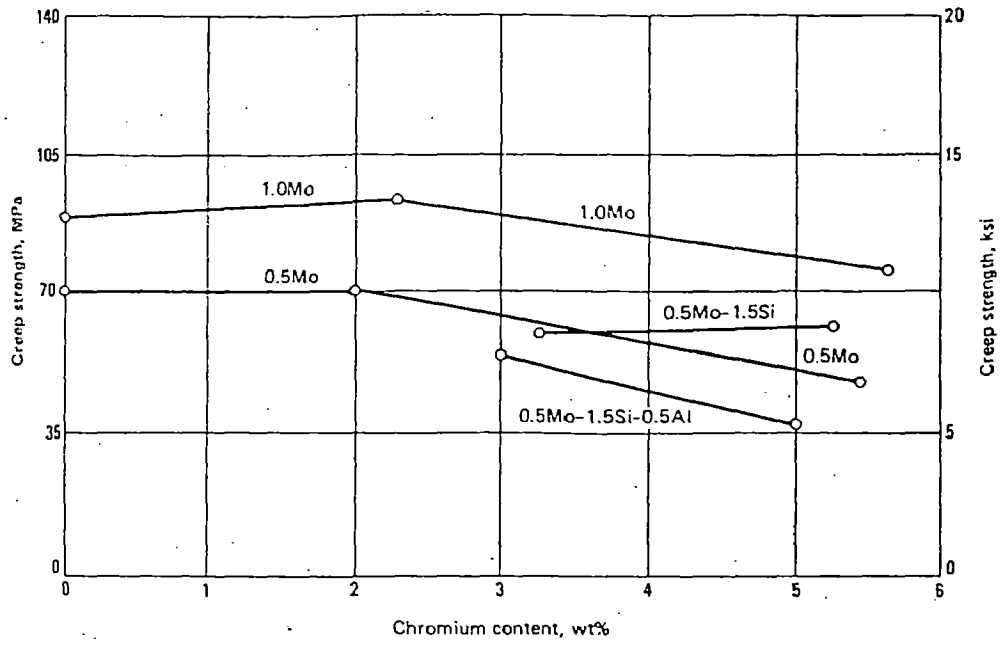


Fig 3-14 Effect of chromium on the creep strength (stress to produce a minimum creep rate of 0.0001% per hour) of several steels containing small amounts of molybdenum, silicon, and aluminum at 540 °C (1000 °F). Source: Ref 68

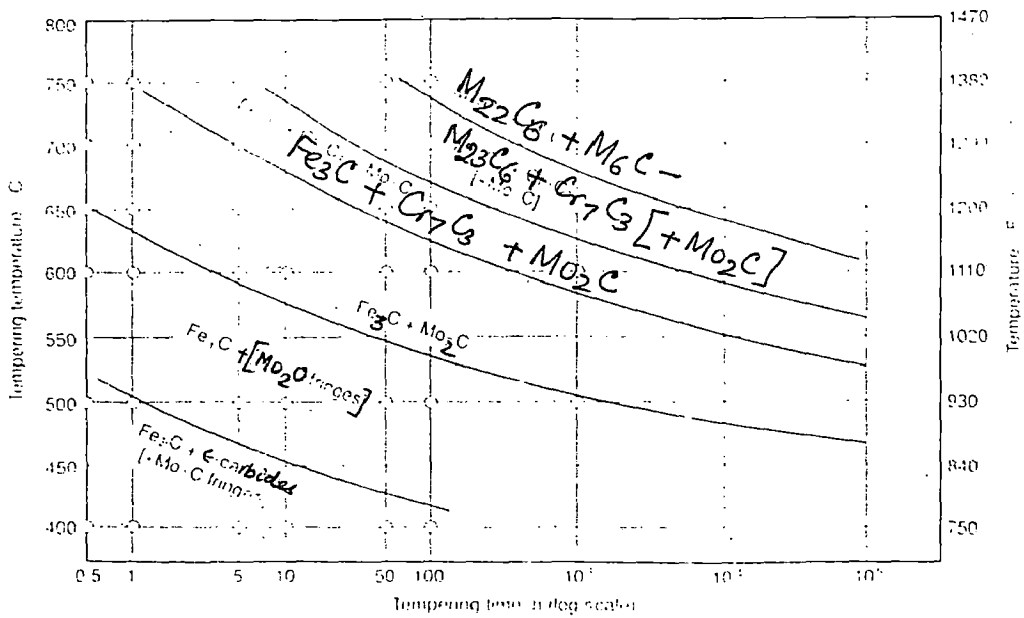


Fig 3-15 Isothermal diagram showing the sequence of carbide formation on tempering of normalized 2 1/4 Cr-1 Mo steel. Source: Ref 12

FIG : Continuous cooling transformation diagram for air-cooled 2¼Cr-1Mo steel (Ref 9)

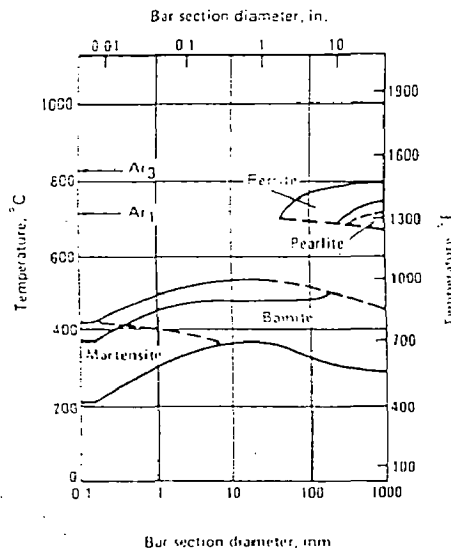
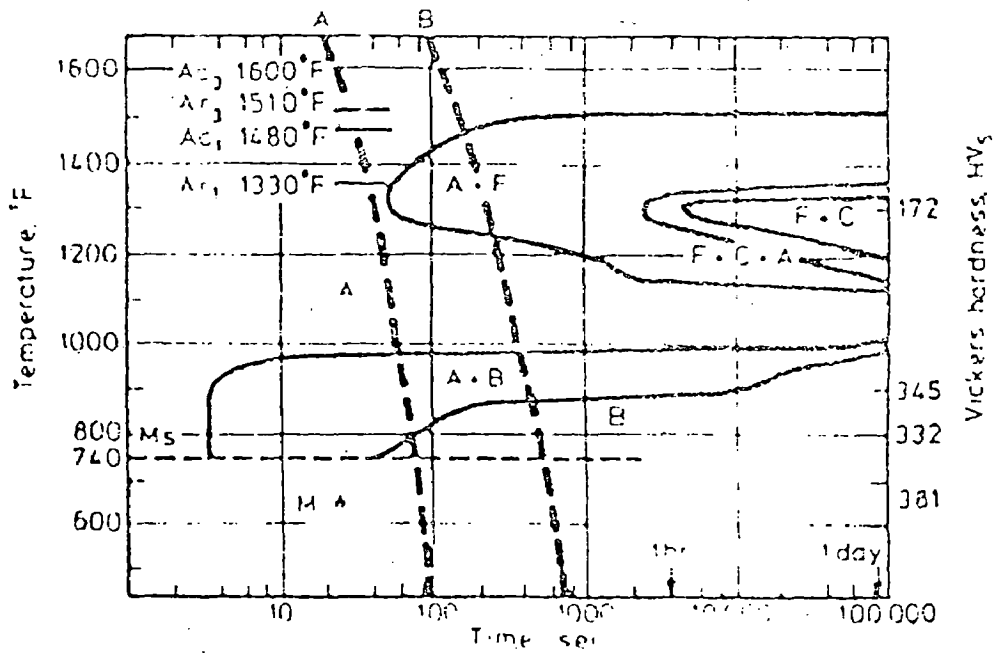
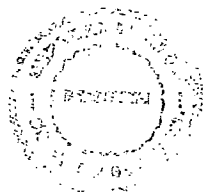


FIG : 3.16

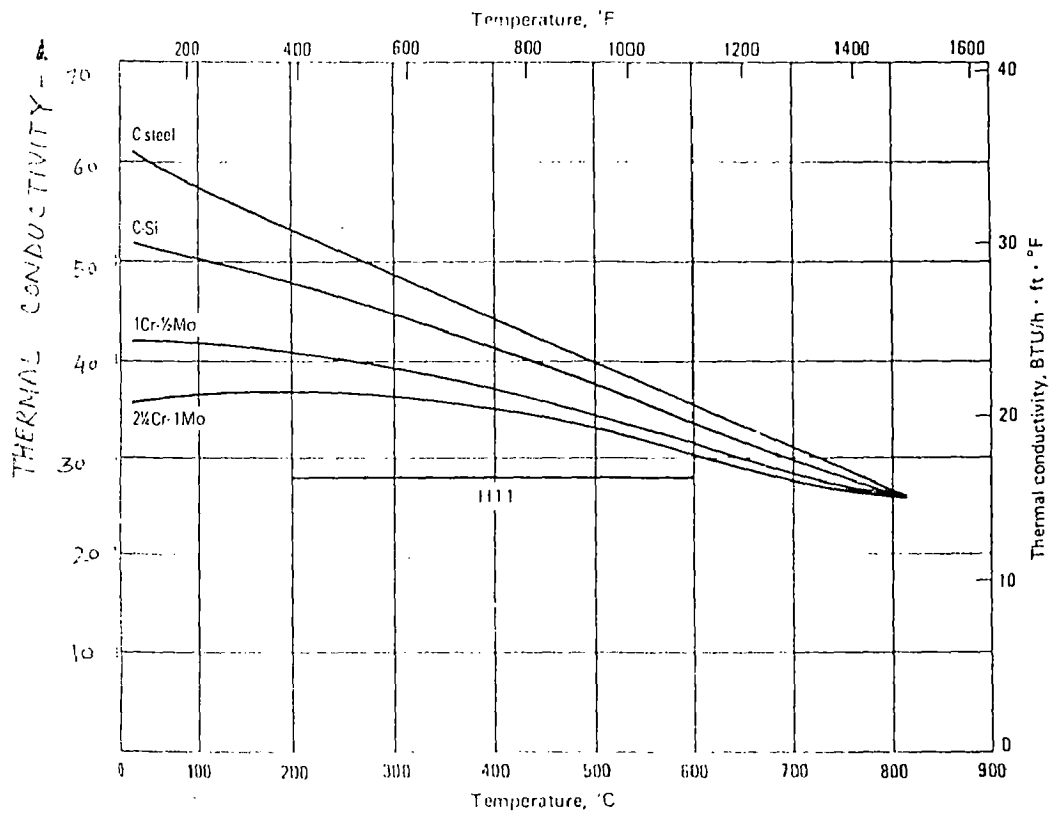


TTT diagram for 0.1C, 0.42Mn, 0.0135S, 0.018P, 0.025Si, 2.16Cr, 0.27Ni, 0.96Mo steel, austenitized at 1860°F for 45min, with cooling rates superimposed

FIG : 3.17

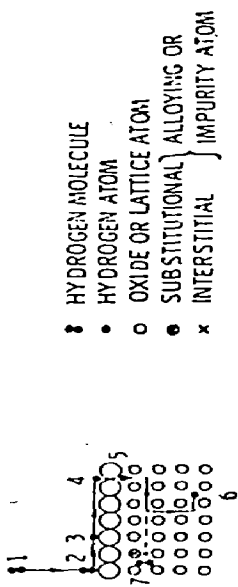


247437



* Thermal conductivity of carbon and low-alloy steels at various temperatures

FIG : 3.18

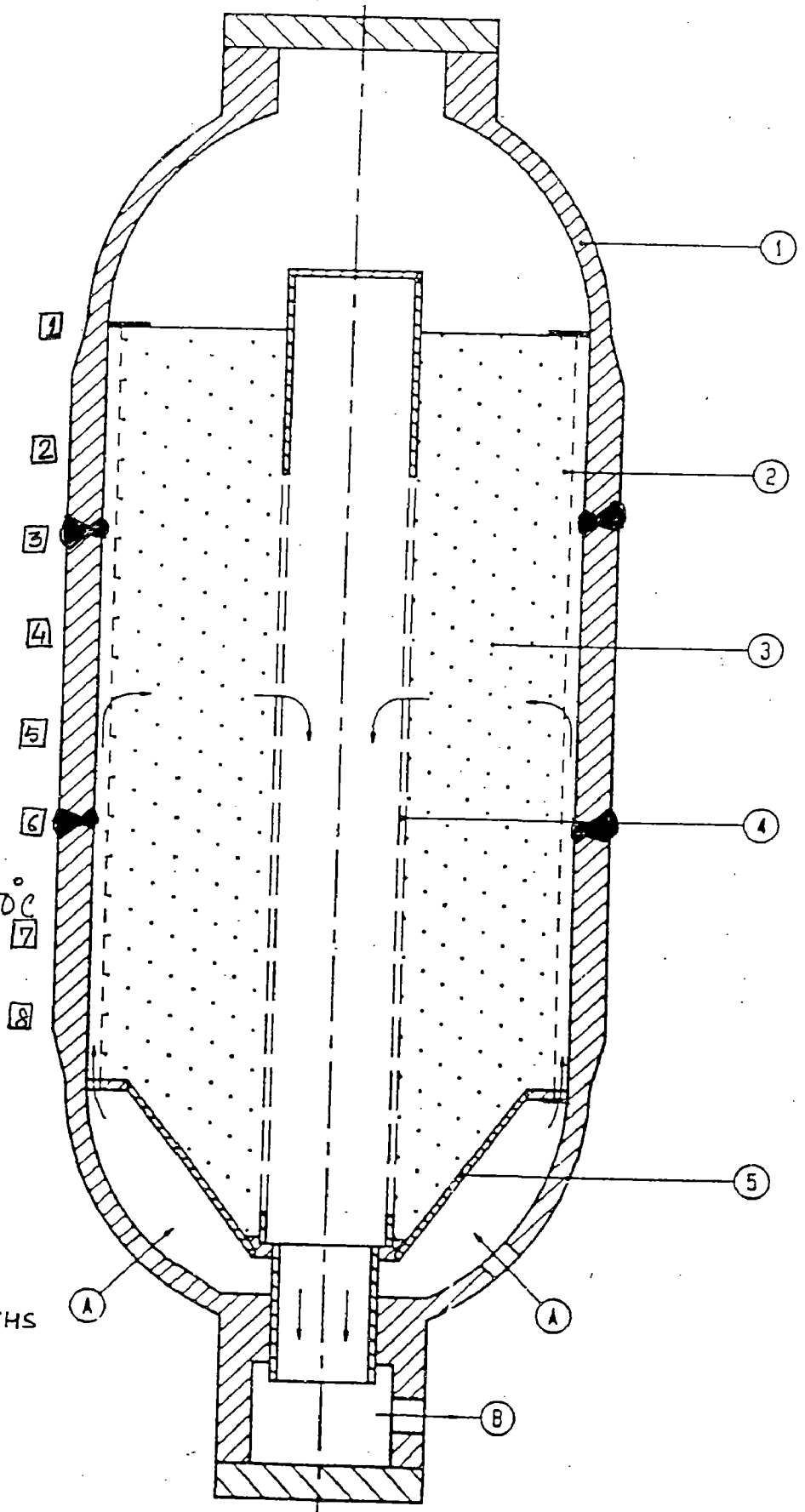


STEPS NECESSARY FOR EMBRITTELEMENT	OCCURRENCE OF EMBRITTELEMENT STEPS		
	HYDROGEN ENVIRONMENT	INTERNAL REVERSIBLE	HYDROGEN REACTION
1→2 MOLECULAR PHYSORPTION	YES	NO	YES/NO
2→3 DISSOCIATION	YES	NO	YES/NO
3→4 CHEMISORPTION	YES	NO	YES/NO
4→5 SOLUTION (ABSORPTION)	YES	YES	YES
5→6 LATTICE DIFFUSION	?	YES	YES/NO
5/6→7 HYDROGEN REACTION TO FORM HYDRIDES AND/OR GAS BUBBLES	NO	NO	YES

FIG. 4—Physical and chemical processes necessary for various types of hydrogen embrittlement [1].

A : GAS INLET
 B : GAS OUTLET

- 1 : PRESSURE SHELL
- 2 : SCREEN PANELS
- 3 : CATALYST BED
- 4 : CENTRE SCREEN
- 5 : CATALYST SUPPORT



Design temp of shell = -450°C

SITE JOINT
 WELD SEAM

SEAM NO. 6 WAS FOUND
 CRACKED AFTER SIX MONTHS
 OF SERVICE.

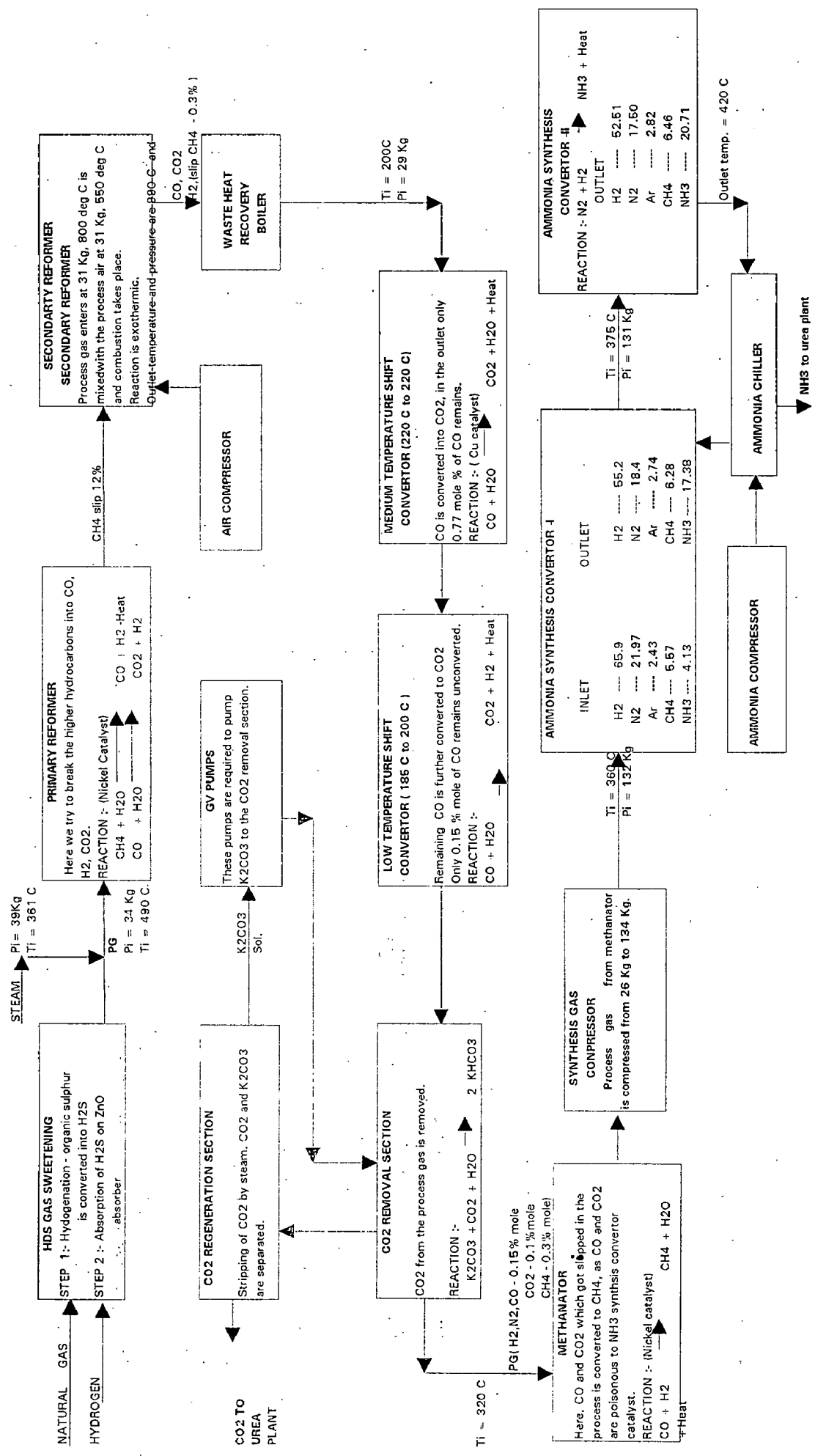


Fig 5-2 : A AMMONIA PLANT PROCESS DIAGRAM

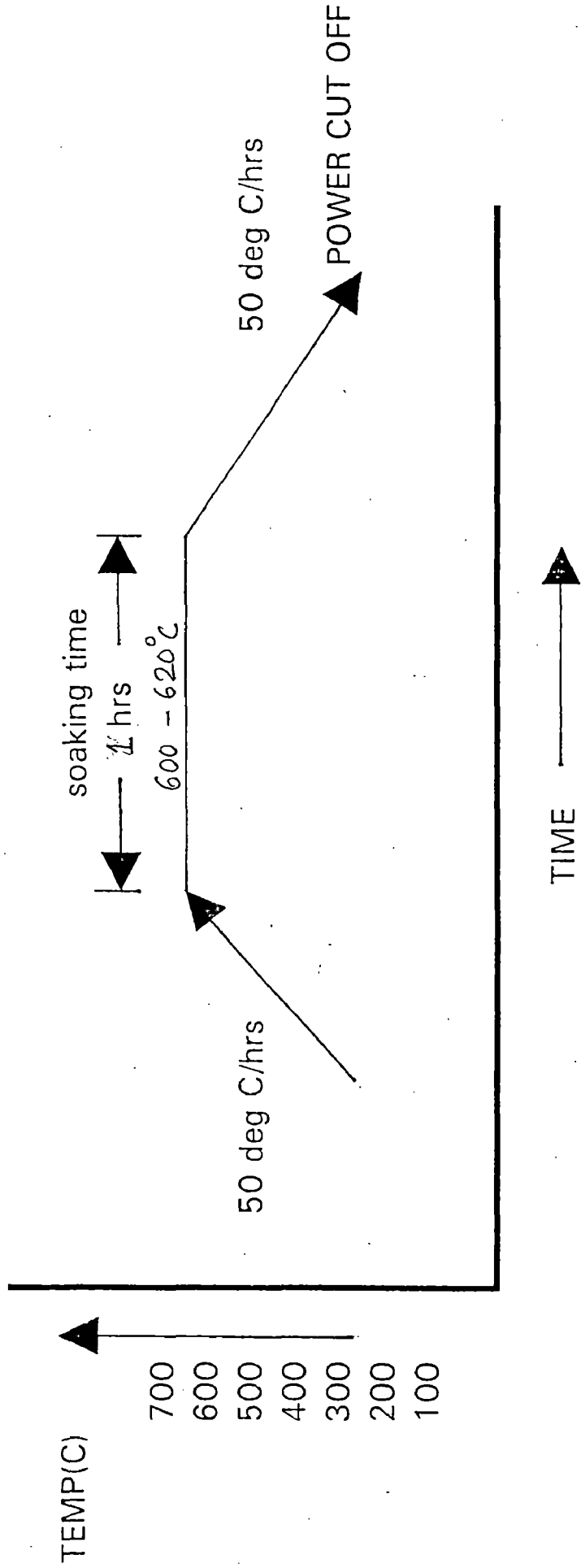


Fig 5.3 : Intermediate stress relieving cycle

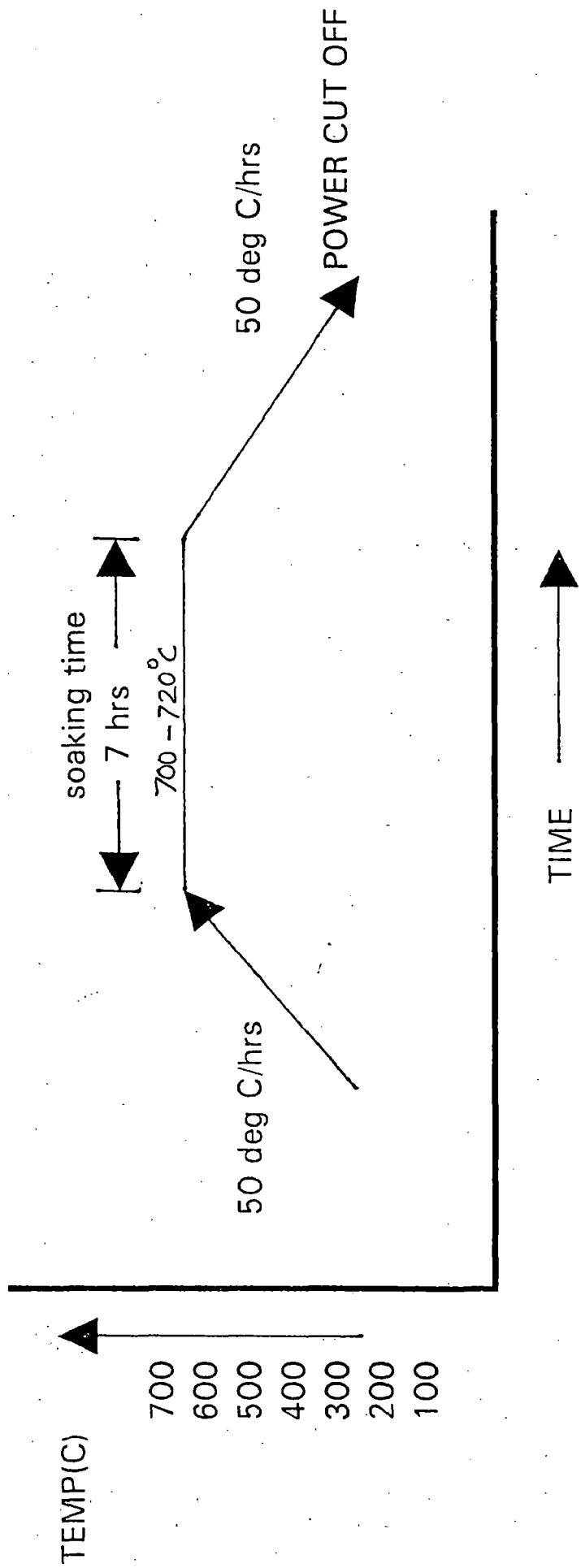


Fig 5.4 : POST WELD HEAT TREATMENT

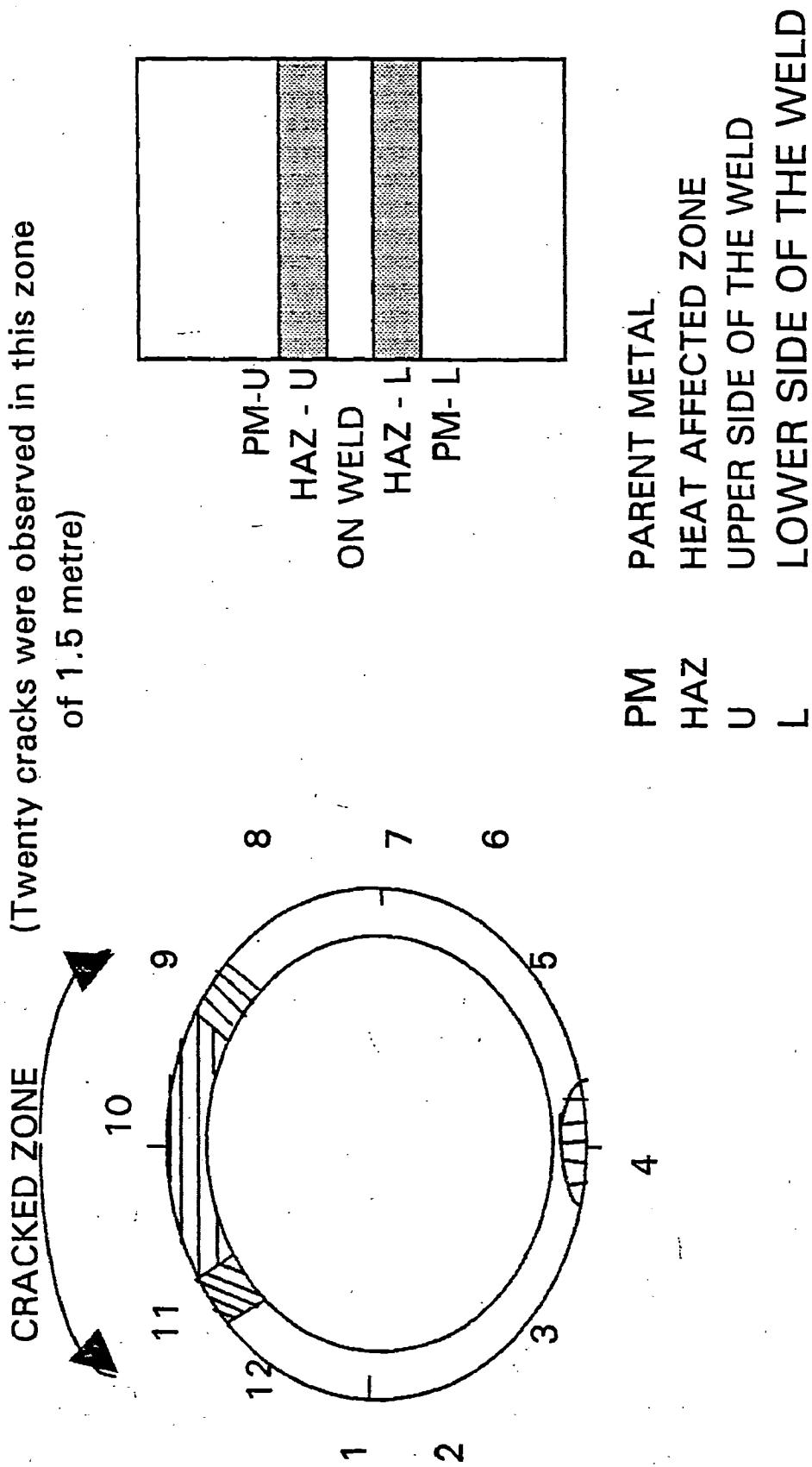
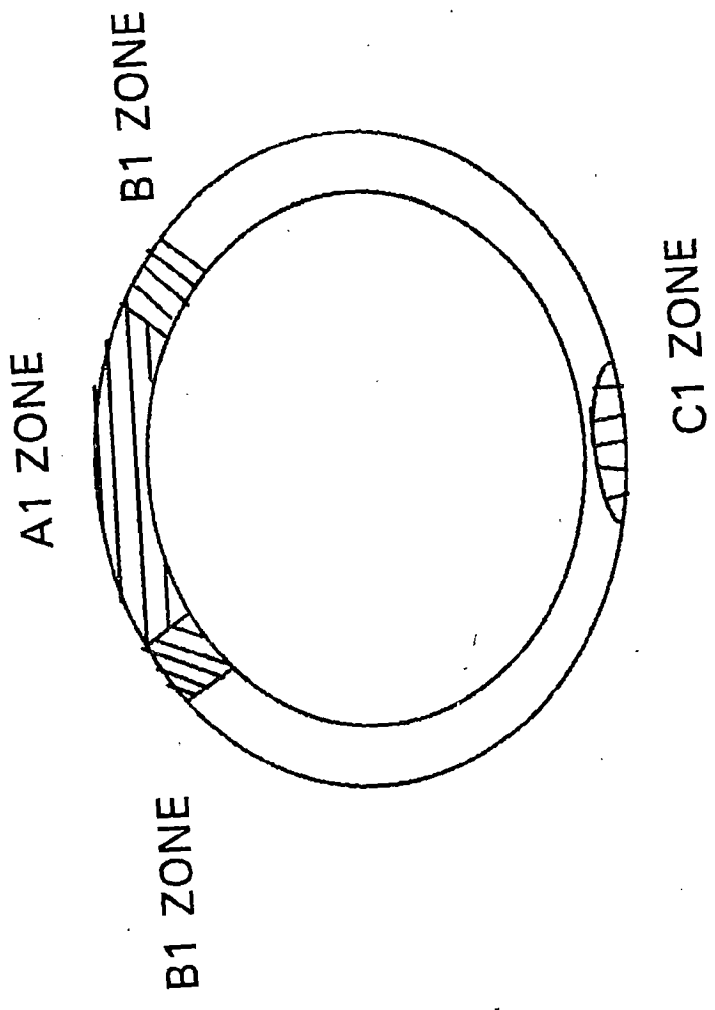


Fig. 5.5 Positions are marked on the weld seam for taking the hardness at various location.



- A1 ZONE : Zone in which cracks were observed.
- B1 ZONE : Zone adjacent to A1 zone.
- C1 ZONE : Zone opposite to A1 zone.

Fig. 5.6 Weld seam showing the location of various zones for further analysis

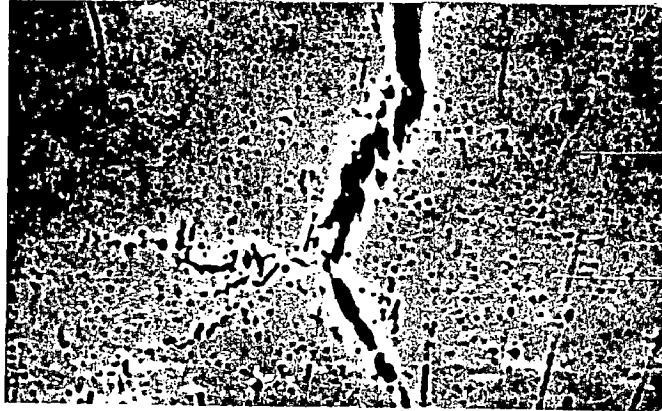


Fig. 5.7 Cracks following course prior austenitic grain boundaries. Porosity is also visible (unetched; X 30).



Fig 5.8 Same as 5.7, but at higher magnification (unetched; X 100).



Fig. 5.9 Cracks following course prior austenitic grain boundaries. Porosity is also visible (unetched; X 30).



Fig. 5.10 Same as Fig. 5.8, but this time after etched in nital (X 100).

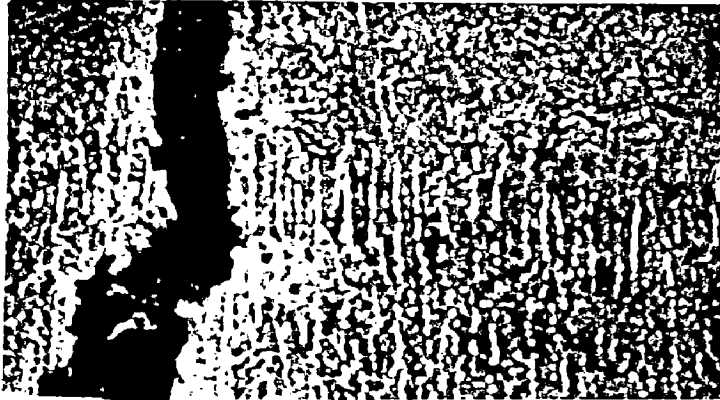


Fig. 5.11 Micrograph showing crack initiating zone, where coarse austenitic grains are visible (Etched in nital; X 100).

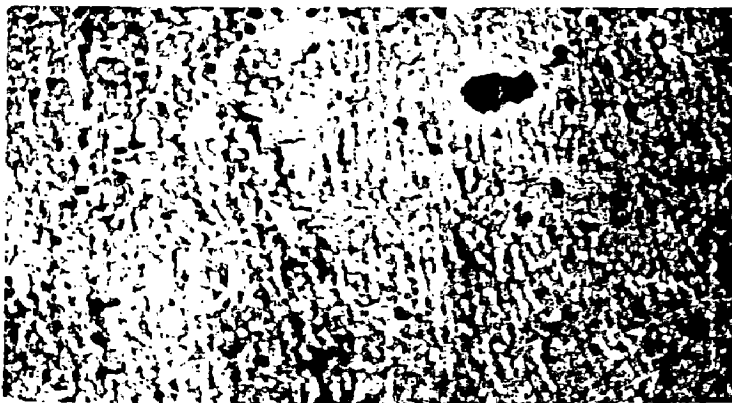


Fig. 5.12 Micrograph away from the crack showing fine prior austenitic grains as compared to coarse grain shown in Fig. 5.11 (Etched in nital; X 100).

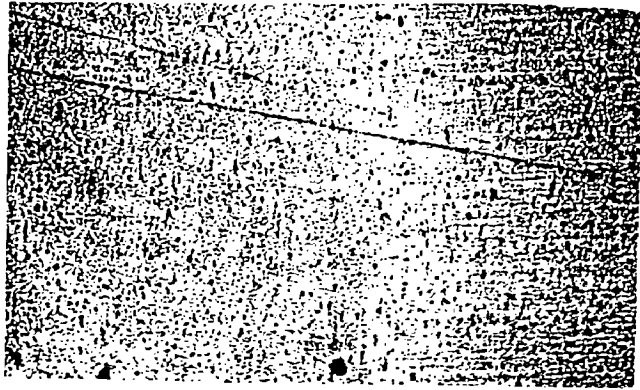


Fig. 5.13 Microstructure of HAZ and weld metal, showing orientation of columnar grains (Etched in nital; X 30).

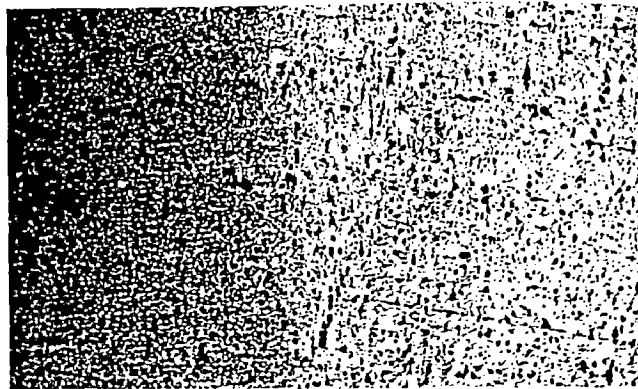


Fig. 5.14 Microstructure of HAZ and parent metal, showing orientation of columnar grains (Etched in nital; X 30).

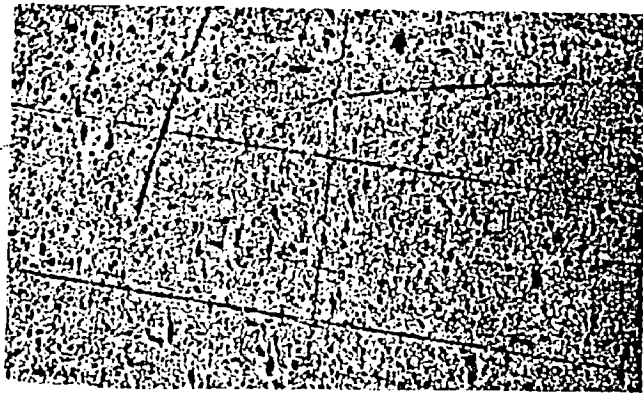


Fig. 5.15 Microstructure of parent metal showing carbide precipitation (Etched in nital; X 30).

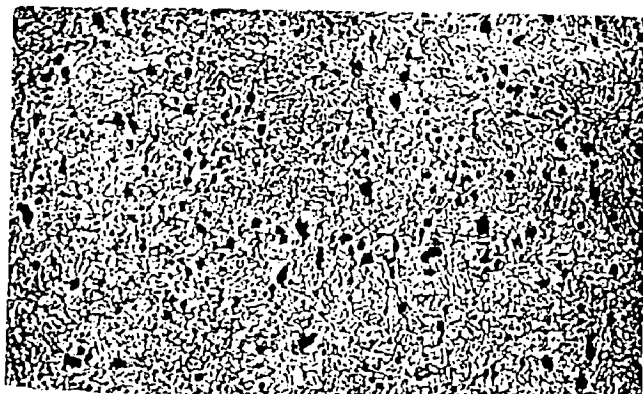


Fig. 5.16 Microstructure of parent metal showing carbide precipitation (Etched in nital; X 100).



Fig. 5.17 Fractograph showing mixture of intergranular cracks, dimple features, tearing & cleavage which has resulted in failure. (160X1.3)



Fig. 5.18 Fractograph showing considerable amount of dimples formed by microvoid coalescence. (160X1.3)

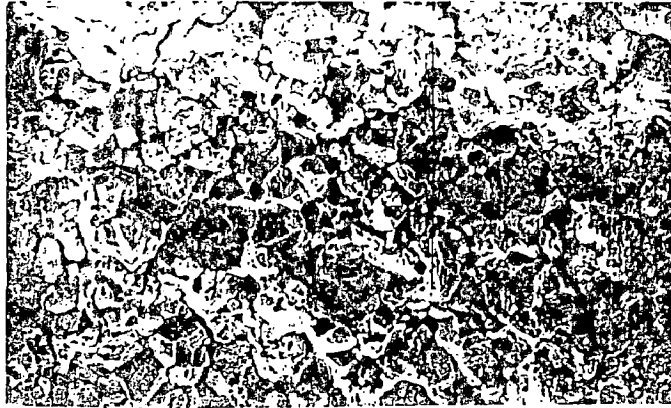


Fig. 5.19 Crack apparently has propagated by mixed mechanism - dimple rupture, intergranular with some evidence of transgranular cracking, and predominant tearing. (160X1.3)

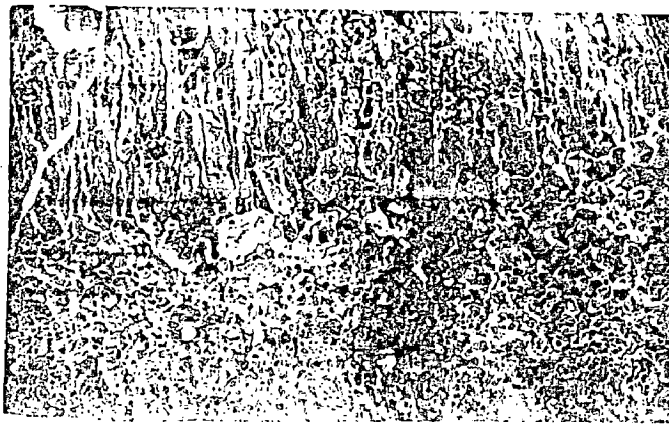


Fig. 5.20 Columnar grains and equiaxed grains. Cracking has occurred mainly by dimple rupture with some sign of tear ridges. (40X1.3)



Fig. 5.21 Enlarged view of Fig. 5.20. This portion of fracture shows transgranular cracks, deep secondary cracks, and hair line indication. Visible are fine ridges, typical of hydrogen embrittlement. (320X1-3)

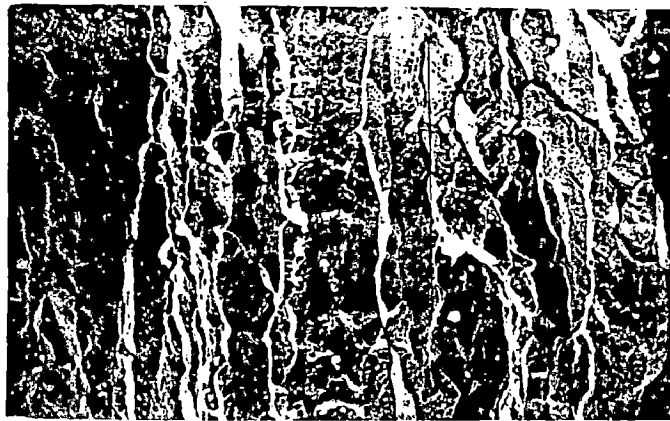


Fig. 5.22 Intergranular cracks with deep secondary cracks between the columnar grains. (160X1-3)



Fig. 5.23 Structure variation observed along the cracked regions. It shows the ductile portion of the fracture surface. At the lower portion, microvoid coalescence is visible. (80X1.4)



Fig. 5.24 Enlarged view of the bottom portion of Fig. 5.23. Channeling which has occurred due to coalescence of voids is visible, surrounded by large tear ridges, secondary cracks are also visible. (160X1.4)

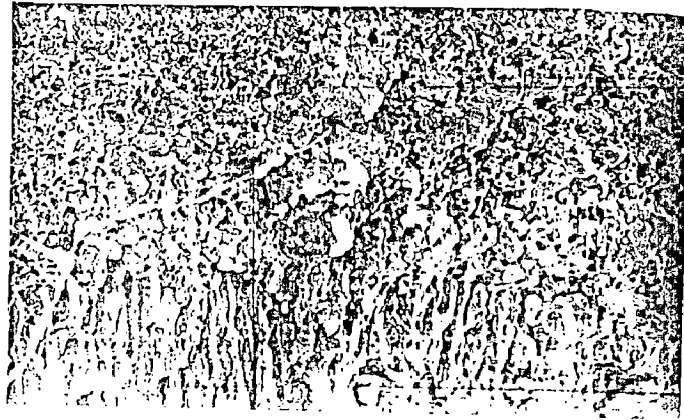
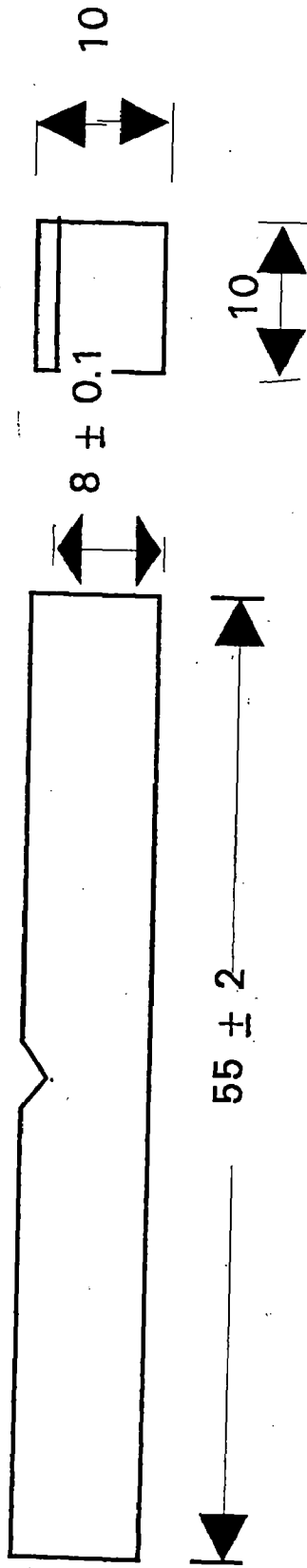


Fig. 5.25 Fractograph showing columnar grains and equiaxed grains. Cracking has occurred mainly by dimples rupture in this region. (40X1.3)



Fig. 5.26 Enlarged view of Fig. 5.24, showing channeling which has occurred due to micro - void coalescence. It also shows large tear ridges. (40X1.3)



Note : All dim in mm

**Fig. 5.27 : STANDARD SAMPLE FOR TOUGHNESS TEST
(CHARPY TEST)**

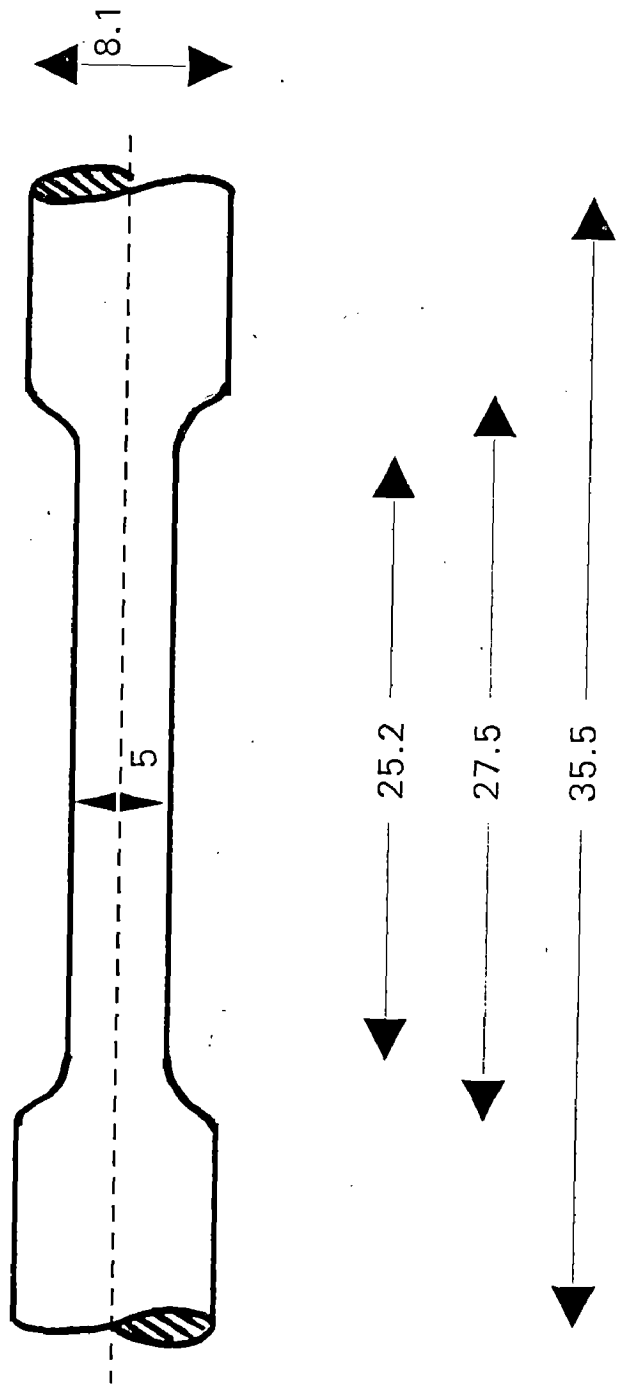


FIG 5-28 : STANDARD TENSILE PIECE SPECIMEN

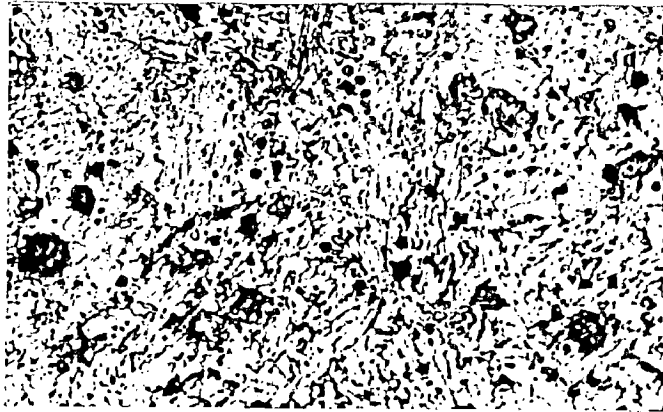


Fig. 5.29 Microstructure of defect free zone (i.e. C_1 zone), showing tempered martensite with some amount of retained austenite (Etched in nital; X 1000).



Fig. 5.30 Same as 4.29 but at different location (Etched in nital; X 1000)

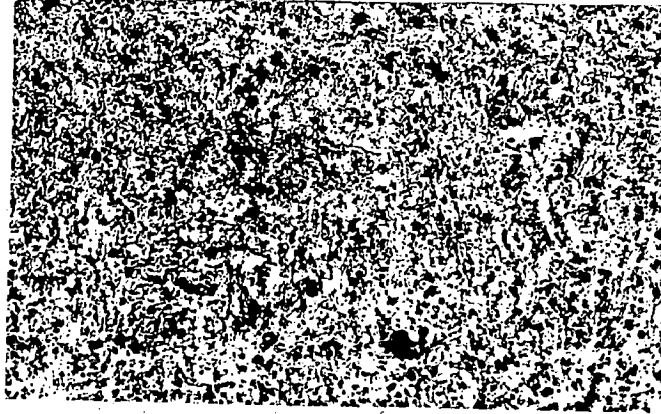


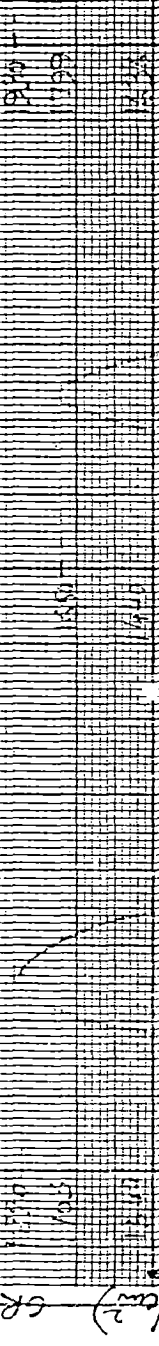
Fig. 5.31 Micrograph of weld zone showing quenched and tempered martensite structure of C₁ zone (Etched in nital; X 200).

STRESS (kg/cm ²)	ELONGATION (%)	STRESS (kg/cm ²)	ELONGATION (%)	STRESS (kg/cm ²)	ELONGATION (%)
1500	15.88	1500	16.2	1500	20
1750	17.2	1750	16.2	1750	20
2000	18.6	2000	16.2	2000	20
2250	20.0	2250	16.2	2250	20
2500	21.4	2500	16.2	2500	20
2750	22.8	2750	16.2	2750	20
3000	24.2	3000	16.2	3000	20
3250	25.6	3250	16.2	3250	20
3500	27.0	3500	16.2	3500	20
3750	28.4	3750	16.2	3750	20
4000	29.8	4000	16.2	4000	20
4250	31.2	4250	16.2	4250	20
4500	32.6	4500	16.2	4500	20
4750	34.0	4750	16.2	4750	20
5000	35.4	5000	16.2	5000	20
5250	36.8	5250	16.2	5250	20
5500	38.2	5500	16.2	5500	20
5750	39.6	5750	16.2	5750	20
6000	41.0	6000	16.2	6000	20
6250	42.4	6250	16.2	6250	20
6500	43.8	6500	16.2	6500	20
6750	45.2	6750	16.2	6750	20
7000	46.6	7000	16.2	7000	20
7250	48.0	7250	16.2	7250	20
7500	49.4	7500	16.2	7500	20
7750	50.8	7750	16.2	7750	20
8000	52.2	8000	16.2	8000	20
8250	53.6	8250	16.2	8250	20
8500	55.0	8500	16.2	8500	20
8750	56.4	8750	16.2	8750	20
9000	57.8	9000	16.2	9000	20
9250	59.2	9250	16.2	9250	20
9500	60.6	9500	16.2	9500	20
9750	62.0	9750	16.2	9750	20
10000	63.4	10000	16.2	10000	20

UTS = 9851 kg/cm²
 % AL = 20%
 % red area = 59.14

UTS = 9716 kg/cm²
 % AL = 16.2%
 % reduction in area = 65%

UTS = 10251 kg/cm²
 % AL = 15.88%
 % red. in area = 51.68



CURVE NO. A
 elongation

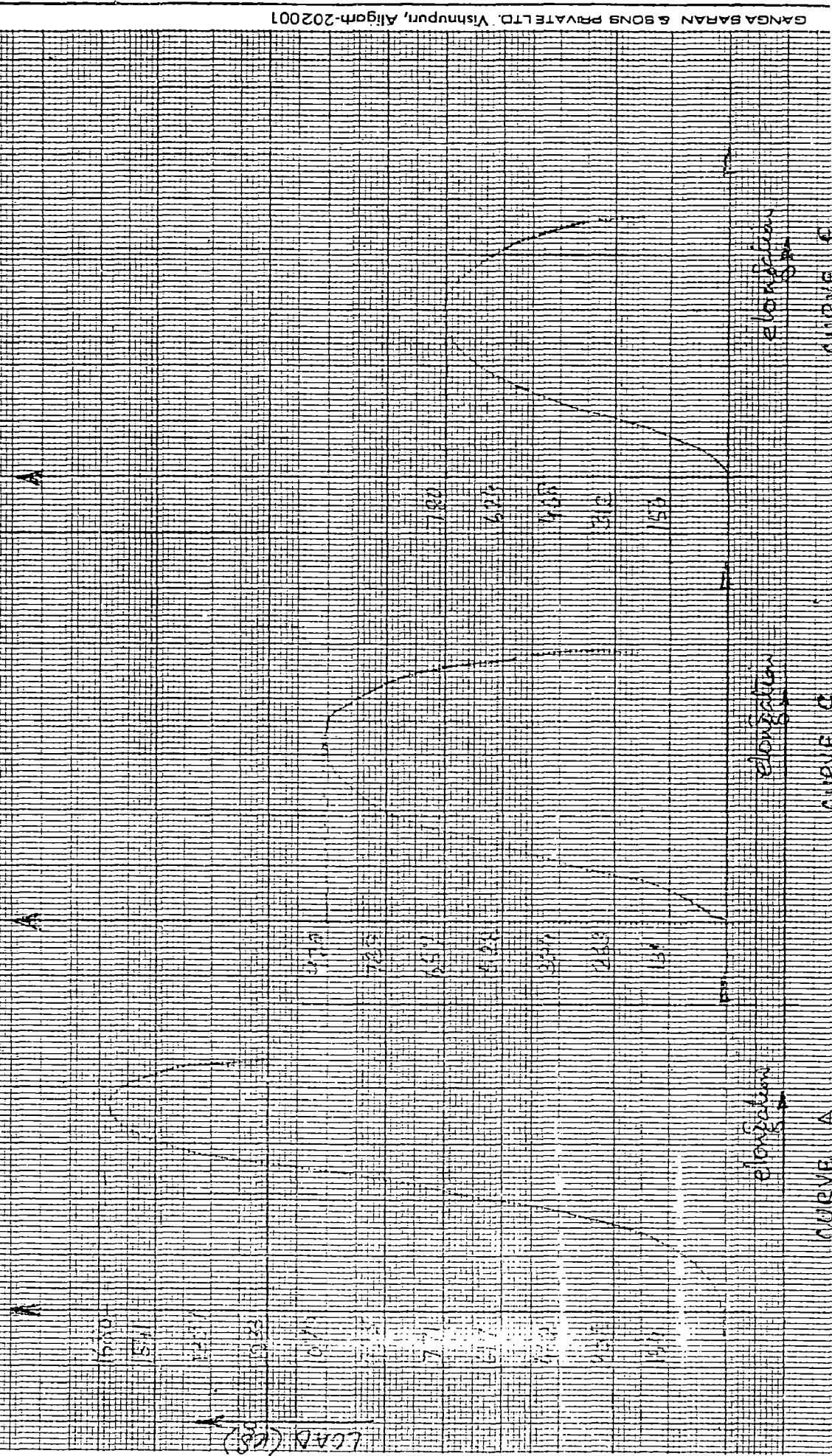
CURVE NO. B
 elongation

CURVE NO. C
 elongation

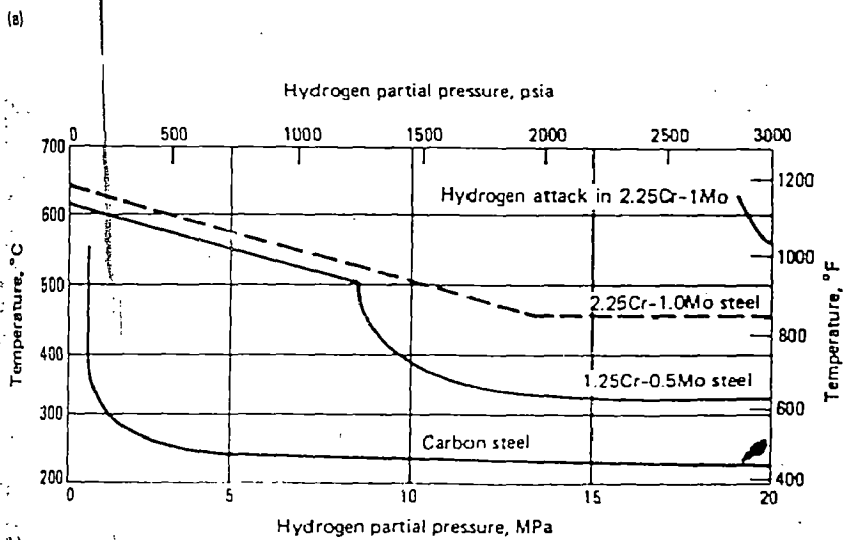
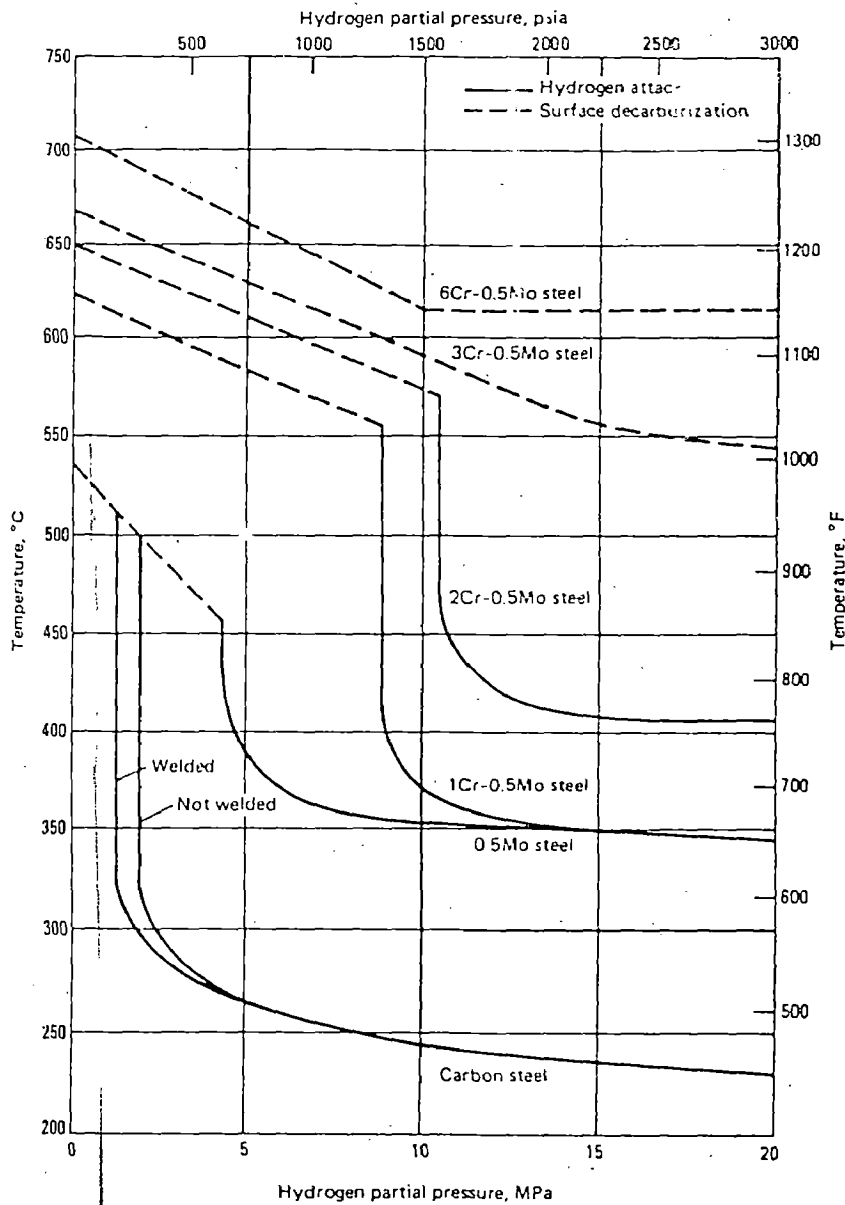
MAX LOAD = 1680 KG
 UTS = 9093 kg/cm²
 % AL = 18.64
 % red. in area = 50.85%

MAX LOAD = 1520 KG
 UTS = 5084 kg/cm²
 % AL = 30.24
 % red. in area = 55.9

MAX LOAD = 150 KG
 UTS = 5369 kg/cm²
 % AL = 32.17
 % red. in area = 50.5



§ 5.33(A) STRESS STRAIN CURVE OF LONGITUDENAL



(a) Nelson curves defining the operating limits of various alloys in a hydrogen environment. Curves adapted from the chart of Nelson. Source: Ref 52. (b) Nelson curves for three steels given in Ref 36 and an estimate of the operating limit (solid line) for the formation of methane bubbles in 2.25Cr-1Mo steel. Source: Ref 53

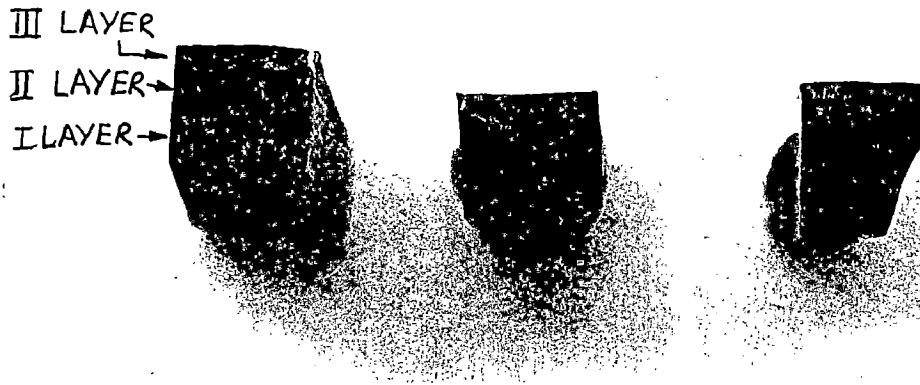


Fig. 5.32 :- Fractured surface of sample piece taken from A₁ zone for SEM analysis.

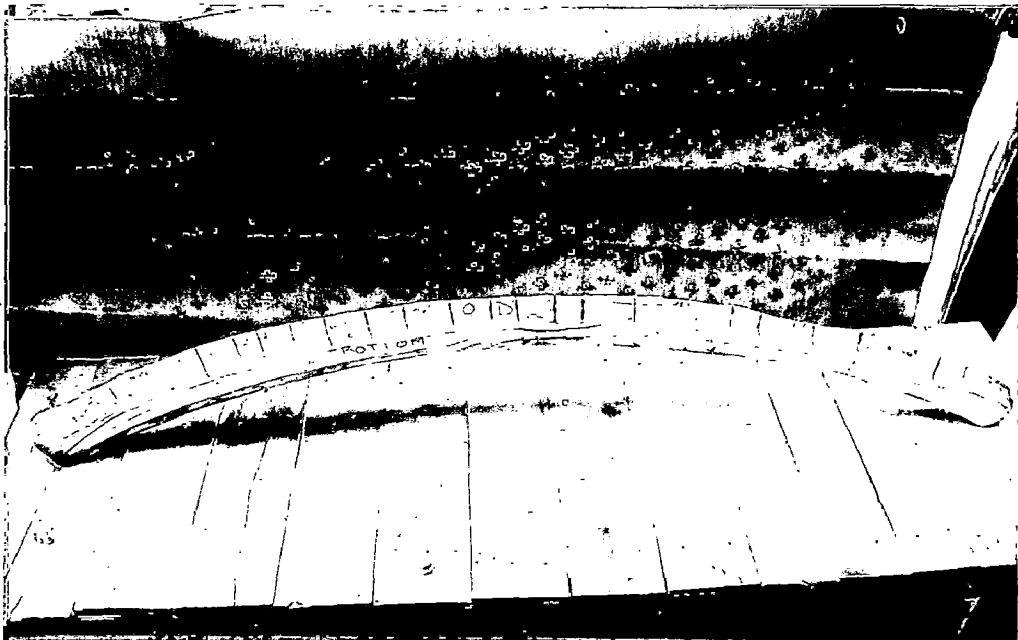


Fig. 5.33 :- A zone of weld₁ seam, where cracks were observed. Photograph is taken after Dye Penetration test. Nineteen distinct radial cracks are visible (Photograph : By country of TCL, Babrala).

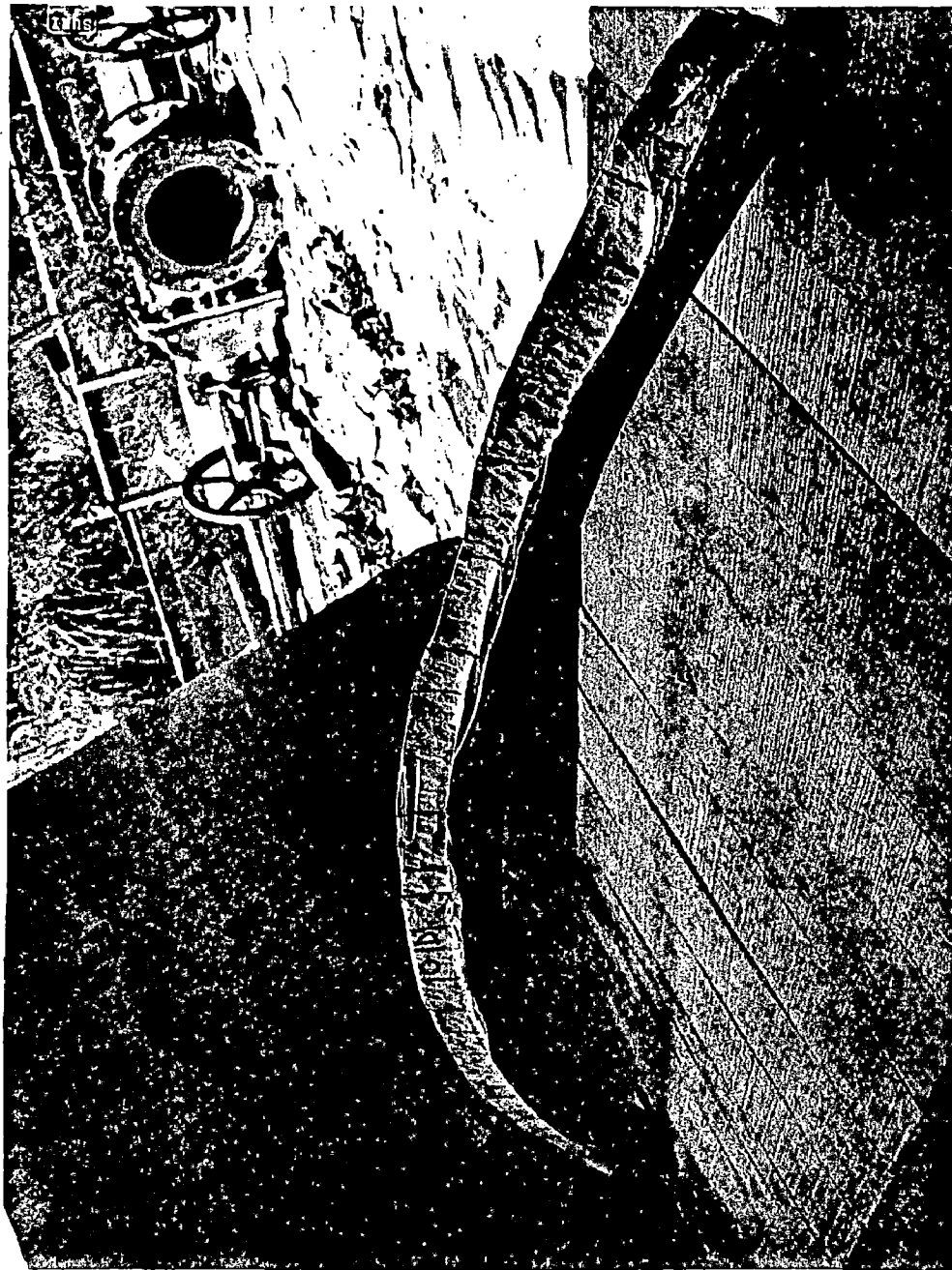


Fig. 5.34 :- Same as Fig. 5.33, but different view.

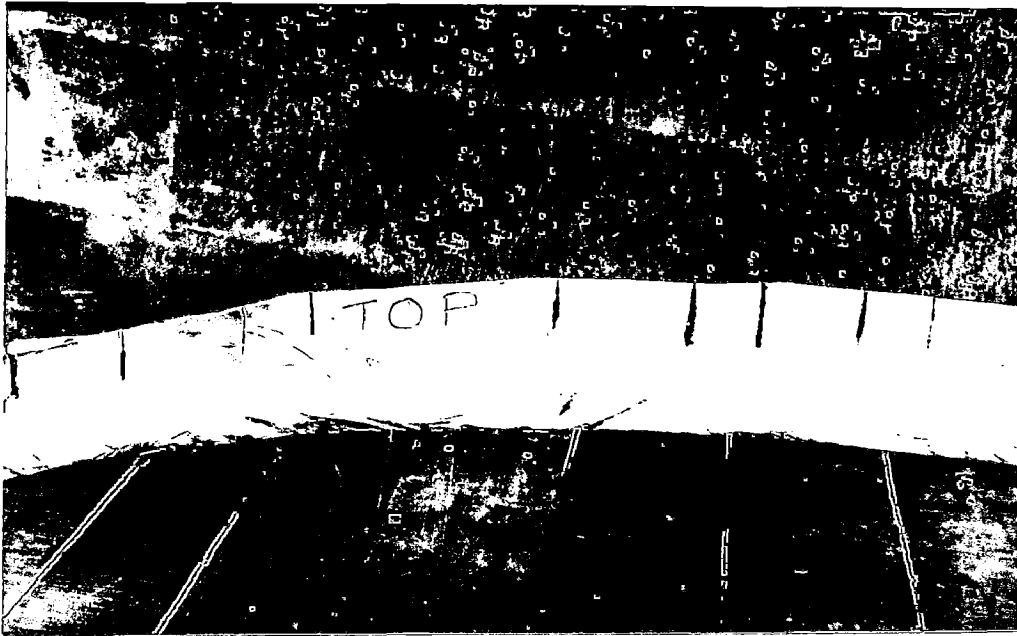


Fig. 5.35 :- Top portion of the segment of weld seam taken from A₁ zone Radial cracks are visible (Photograph : By country of TCL. Babrala).



Fig. 5.36 :- Photograph of the segment of weld seam showing its inner dia with clear visible longitudinal cracks (Photograph : By country of TCL, Babrala).

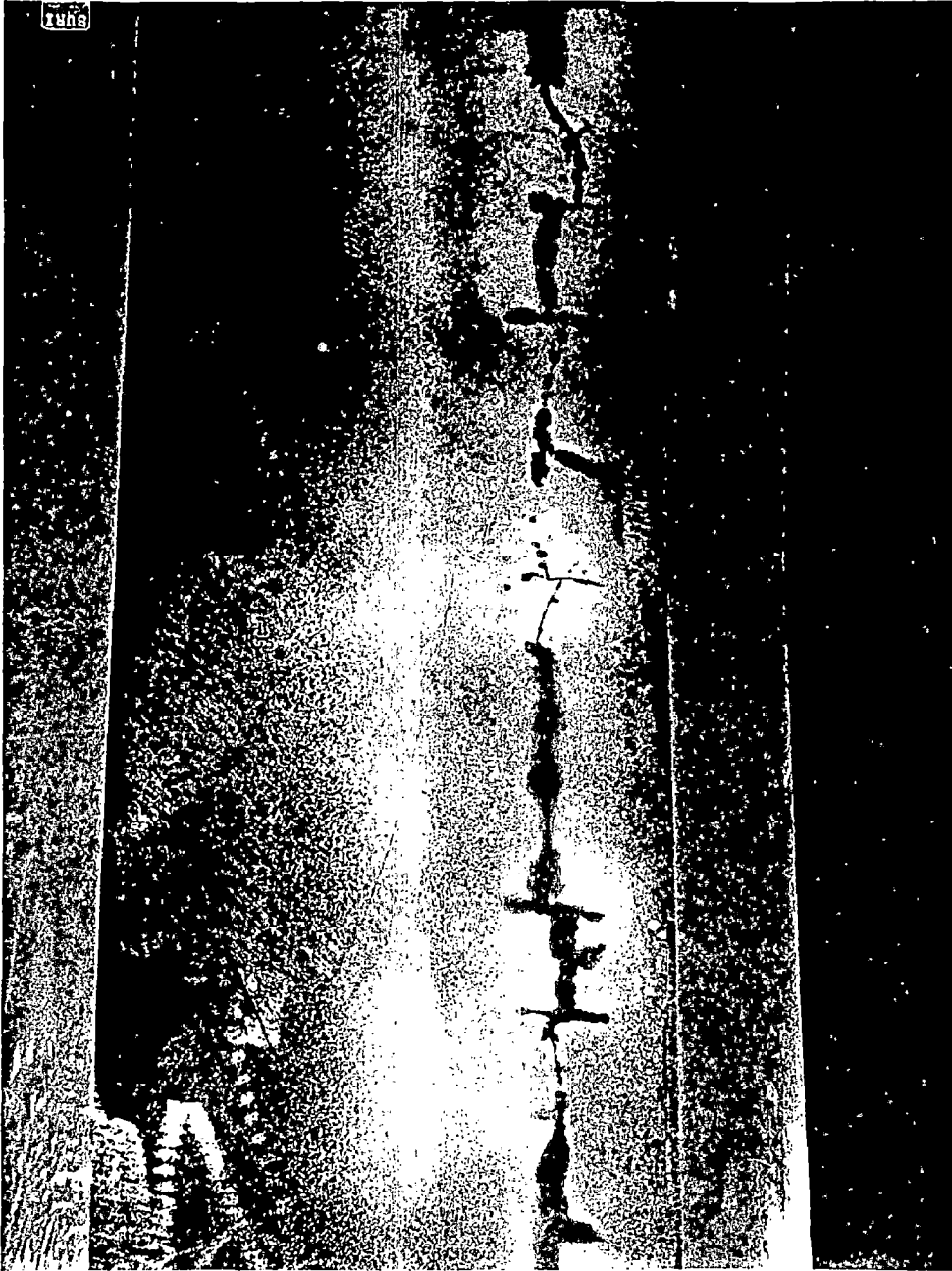


Fig. 5.37 :- Photograph of the weld seam taken from internal reactor surface showing longitudinal and transverse cracks (Photograph : By country of TCL, Babrala).

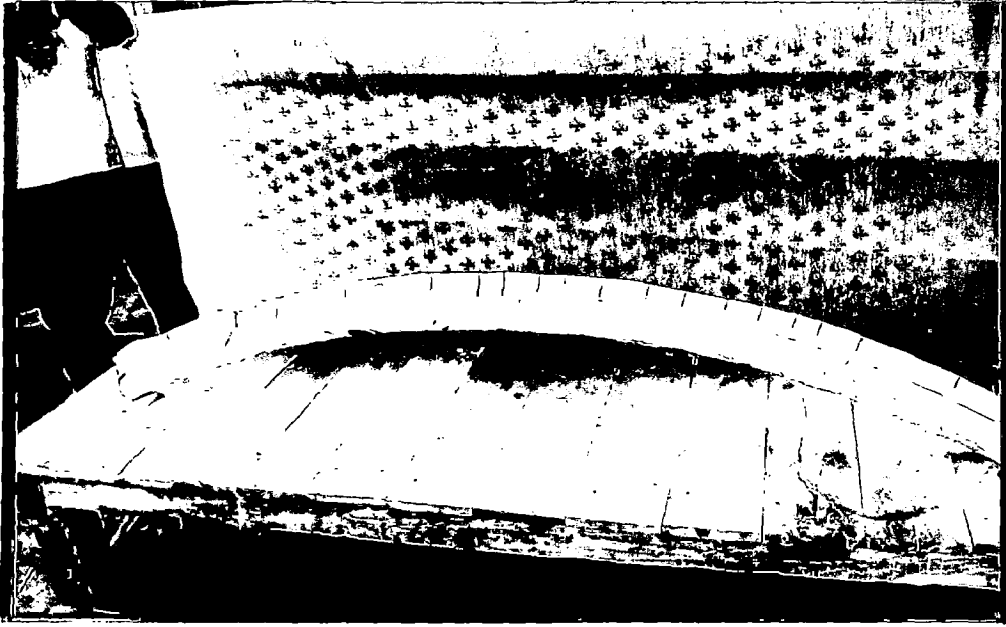


Fig. 5.38 :- Top portion of the segment of weld seam from A_1 zone.
Showing twenty radial cracks (Photograph : By country
of TCL, Babrala).



TABLE 3.1. Nominal chemical compositions chromium-molybdenum steels

Type	Composition, percent ^a						
	C	Mn	S	P	Si	Cr	Mo
1/2Cr-1/2Mo	0.10-0.20	0.30-0.60	0.045	0.045	0.10-0.30	0.50-0.80	0.45-0.65
1Cr-1/2Mo	0.15	0.30-0.60	0.045	0.045	0.50	0.80-1.25	0.45-0.65
1-1/4Cr-1/2Mo	0.15	0.30-0.60	0.030	0.045	0.50-1.00	1.00-1.50	0.45-0.65
2Cr-1/2Mo	0.15	0.30-0.60	0.030	0.030	0.50	1.65-2.35	0.45-0.65
2-1/4Cr-1Mo	0.15	0.30-0.60	0.030	0.030	0.50	1.90-2.60	0.87-1.13
3Cr-1Mo	0.15	0.30-0.60	0.030	0.030	0.50	2.65-3.35	0.80-1.06
5Cr-1/2Mo	0.15	0.30-0.60	0.030	0.030	0.50	4.00-6.00	0.45-0.65
7Cr-1/2Mo	0.15	0.30-0.60	0.030	0.030	0.50-1.00	6.00-8.00	0.45-0.65
9Cr-1Mo	0.15	0.30-0.60	0.030	0.030	0.25-1.00	8.00-10.00	0.90-1.10

a. Single values are maximum

S. NO.	ELEMENT	FLOW N - m ³ /hr	mole %
1	Hydrogen	394716	65.9
2	Nitrogen	131572	21.97
3	Argon	14597	2.43
4	Methane	33346	5.57
5	Ammonia	24725	4.13
	TOTAL	598936	100

Partial Pressure of H₂ :-

$$p = \frac{136 \times 65.9}{100}$$

$$= 89.62 \text{ Kg /cm}^2$$

OR

$$8.962 \text{ MPa}$$

Table 5.1 : Composition of Synthesis gas which enters NH₃ synthesis convertor

JOINT NO-6 (OUTSIDE)

POINT NO	PM-U	HAI-U	ON WELD	HAI-L	PM-L
01.	256	290	280	312	258
	250	278	272	320	241
	241	268	276	311	260
02.	229	289	282	310	286
	260	276	276	300	298
	248	290	296	321	276
03.	302	278	268	288	275
	290	260	284	282	286
	295	290	274	276	292
04.	250	225	286	262	229
	218	215	294	250	236
	222	230	268	242	216
05.	231	226	271	245	248
	248	210	268	235	239
	239	230	258	225	250
06.	241	235	279	251	216
	220	212	252	241	230
	230	225	263	235	225
07.	221	229	252	236	229
	214	252	246	252	220
	232	239	245	222	235
08.	321	315	318	340	284
	214	305	320	329	276
	212	296	303	335	272
09.	318	300	*258	323	339
	322	312	MIDWALL	212	320
	330	290	HARDNESS	230	315
10.	308	268		308	312
	300	298		296	305
	315	296		298	290
11.	271	336	*265	302	241
	250	352	MIDWALL	298	235
	268	320	HARDNESS	282	225
12.	330	236	268	289	239
	328	212	286	268	234
	215	224	260	294	223

NOTE :-ALL MEASUREMENTS ARE IN BHN

TABLE 5.2

Hardness values obtained from outside the vessel.

JOINT NO-6 (INSIDE)

POINT NO	PM-U	HAI-U	ON WELD	HAI-L	PM-L
01.	174	181	179	167	174
	184	189	184	160	182
	188	188	164	159	166
02.	174	169	202	165	184
	178	172	196	172	176
	184	172	198	156	170
03.	168	177	167	154	164
	174	160	174	166	176
	164	168	184	156	168
04.	190	177	179	175	172
	200	188	176	184	186
	198	172	180	198	180
05.	158	168	156	163	160
	174	174	166	174	182
	160	180	158	180	176
06.	176	181	198	186	186
	180	184	202	160	174
	194	178	198	177	186
07.	184	159	206	179	174
	178	165	201	186	164
	184	150	196	176	168
08.	180	179	215	200	170
	188	184	201	184	174
	186	196	208	194	168
09.	164	177	198	161	174
	166	181	189	170	174
	164	189	192	156	170
10.	176	194	196	190	160
	166	201	188	186	174
	178	193	196	186	168
11.	154	215	202	203	172
	142	208	201	208	170
	158	196	198	212	180
12.	168	173	182	179	190
	174	185	186	188	198
	176	178	170	194	188

OTE :- ALL MEASUREMENTS ARE IN BHN

TABLE 5.3 *Hardness values obtained from inside the vessel.*

TRANSVERSE SAMPLES B(T):

S.NO	DIAGONAL D(1)	DIAGONAL D(2)	AVERAGE DIAGONAL	VHN
1	0.392	0.392	0.392	362
2	0.393	0.393	0.393	360
3	0.412	0.414	0.413	326
4	0.391	0.389	0.39	366
1	0.391	0.389	0.39	366
2	0.389	0.387	0.388	370
3	0.418	0.414	0.416	312

SAMPLE 1

SAMPLE 2

LONGITUDENAL SAMPLES B(L):

S.NO	DIAGONAL D(1)	DIAGONAL D(2)	AVERAGE DIAGONAL	VHN
1	0.429	0.428	0.4285	302
2	0.425	0.418	0.4215	313
3	0.526	0.519	0.5225	204
4	0.526	0.521	0.5235	203
1	0.51	0.508	0.509	215
2	0.449	0.449	0.449	276
3	0.465	0.462	0.4635	259

SAMPLE 1

SAMPLE 2

FORMULA USED :-

$$\text{VHN} = \frac{1.854 \times W}{D \times D} \text{ kg /cm}^2$$

Table 5.4:- Hardness values of transverse and longitudinal direction of sample piece taken from zone B1

S.NO	CROSS-SCETION AREA BELOW THE NOTCH (cm2)	IMPACT ENERGY ABSORBED (Kg - m)	NOTCH IMPACT	
			STRENGTH (Kg - m /cm2)	
1	9.8 x 8.2	8.6	10.7	
2	9.8 x 8	9.47	12.08	
3	9.8 x 8.1	7.65	9.64	
4	9.8 x 8.1	6.49	8.18	

TRANSVERSE {
SAMPLE
LONGITUDENAL {
SAMPLE

Table 5.5 :- Results of charpy test performed on sample piece taken from B1 zone

LONGITUDINAL PIECE

S.NO.	SAMPLE DIA (MM)	GAUGE LENGTH (MM)	CHANGED LENGTH (MM)	MAX. LOAD Kg/cm ²	BREAKING LOAD Kg/cm ²	UTS Kg/cm ²	% ELONG
1	4.85	19.05	22.6	1680	1260	9093	18.64
2	4.8	20.5	26.7	920	420	5084	26.7
3	4.3	21.8	28.8	780	330	5371	32.1

TRANSVERSE PIECE

S.NO.	SAMPLE DIA (MM)	GAUGE LENGTH (MM)	CHANGED LENGTH (MM)	MAX. LOAD Kg/cm ²	BREAKING LOAD Kg/cm ²	UTS Kg/cm ²	% ELONG
1	4.85	21.6	25.6	1820	1230	9851	19.9
2	4.65	21.45	21.7	1650	1320	9716	
3	4.9	21.4	24.8	1930	1580	10231	15.88

Table 5.6 : TENSILE TEST FOR B(1) ZONE

CHEMICAL ANALYSIS REPORT

ELEMENTS	CARBON	CHROMIUM	NICKEL	MOLYBDENUM	NIOBIUM	VANADIUM
%	0.11	2.64	1.93	0.96	0.02	-

Table : Chemical analysis of A1 zone

ELEMENTS	CARBON	CHROMIUM	NICKEL	MOLYBDENUM	NIOBIUM	VANADIUM
%	0.12	2.4	1.99	0.99	-	-

Table : Chemical analysis of B1 zone

ELEMENTS	CARBON	CHROMIUM	NICKEL	MOLYBDENUM	NIOBIUM	VANADIUM
%	0.1	2.33	2.03	0.96	-	-

Table : Chemical analysis of C1 zone

Table 5-7 :- CHEMICAL ANALYSIS REPORT OF SAMPLES OF VARIOUS ZONES

S.NO	DIAGONAL	DIAGONAL	DIAGONAL	AVERAGE	VHN
	D(1)	D(2)		DIAGONAL	
1	0.462	0.471		0.466	256
2	0.441	0.449		0.445	281
3	0.447	0.438		0.442	285
4	0.46	0.458		0.459	264

FORMULA USED :-

$$\text{VHN} = \frac{1.854 \times W}{D \times D} \text{ Kg / cm}^2$$

Table 5.8 :- Hardness values of sample piece taken from C1 zone

ASME SPECIFICATION	GRADE	YIELD STRENGTH	UTS	Minimum elongation in	Minimum reduction in
		(Kg / cm ²)		50 mm, (%)	area, %
SA 387	Gr 22 class 1	2050	4150 -5850	45	40
SA 387	Gr 22 class 2	3100	5150 - 6900	45	40

Table 5.9:- Room temperature mechanical properties of 2.25 % Cr - 1% Mo steel

CHEMICAL ANALYSIS

ELEMENTS	CARBON	CHROMIUM	MOLYBDENUM	SILICON	PHOSPHORUS	SULPHUR
%	0.04 -0.15	1.88 -2.62	0.85 -1.15	0.5 MAX	0.035	0.035

Table 5.10 : Standard Chemical composition of A 387 Gr 22 cl 2 plates as per ASTM standards

REFERENCES

1. HANS R. KAUTZ and HERBERT E.D. ZURN, "Materials & Welding in Power Plants".
2. ASM vol.1, "Elevated temperature properties of Ferritic steels", pp. 617 - 651.
3. E.C. ROLLASON, "Metallurgy for Engineers", ELBS, Fourth edition (1986).
4. V. Raghvan, "Physical Metallurgy".
5. ROBERT BRUSCATO, "Temper Embrittlement and Creep Embrittlement of 2.25 Cr - 1 Mo shielded Metal Arc Weld Deposits", WJ April 1970, pp. 148-s to 156-s.
6. N.S. CHERUVU, "Degradation of Mechanical Properties of Cr-Mo-V and 2.25 Cr - 1 Mo Steel Components After Long - Term Service at Elevated Temperatures", Metallurgical Transactions, Vol. 20A, Jan 89, pp. 87 - 97.
7. J.GROSSE - WORDEMANN AND S. DITTRICH, "Prevention of Temper Embrittlement in 2 1/4 Cr - 1 Mo Weld metal by Metallurgical Actions", WJ May 1983, pp. 1245 - 1285.
8. J.G. Zhang, F.W. Noble and B.L. Eyre, "Comparison of Effects of aging on fracture of 9 Cr - 1 Mo & 2.25 Cr - 1 Mo Steel, Part 1 Quenched and Tempered Material", Material Science & Technology, March 1991, Vol.7, pp.218 - 223.
9. Welding Handbook, Vol. 4, "Metals & Their Weldability".
10. R. GIBALA & R.F. HEHEMANN, "Hydrogen Embrittlement and Stress

Corrosion Cracking".

11. LI RENSHUN & WU RENGENG, "Study on improving the resistance of high strength steel to hydrogen embrittlement.
12. KENNETH EASTERLING, "Introduction to the Physical Metallurgy of Welding.
13. ASM Vol. 1, 10th edition, "Cracking Phenomenon Associated with Welding".
14. ASM Vol. 6, 10th edition, "Welding, Brazing & Soldering".
15. Metals Handbook, ASM Vol. 7, 8th edition, "Fractography and atlas of fractographs.
16. LANCHESTER, "Metallurgy of Welding".
17. Process Manual of AMMONIA PLANT of TCL, Babrala.
18. Metal Handbook, "Descaling & Cleaning of SS and heat resistant Alloys", pp. 29.7 - 29.42.
19. ASM Vol. 10, 8th edition, "Failure analysis & Prevention".